CHALMERS
UNIVERSITY OF TECHNOLOGY

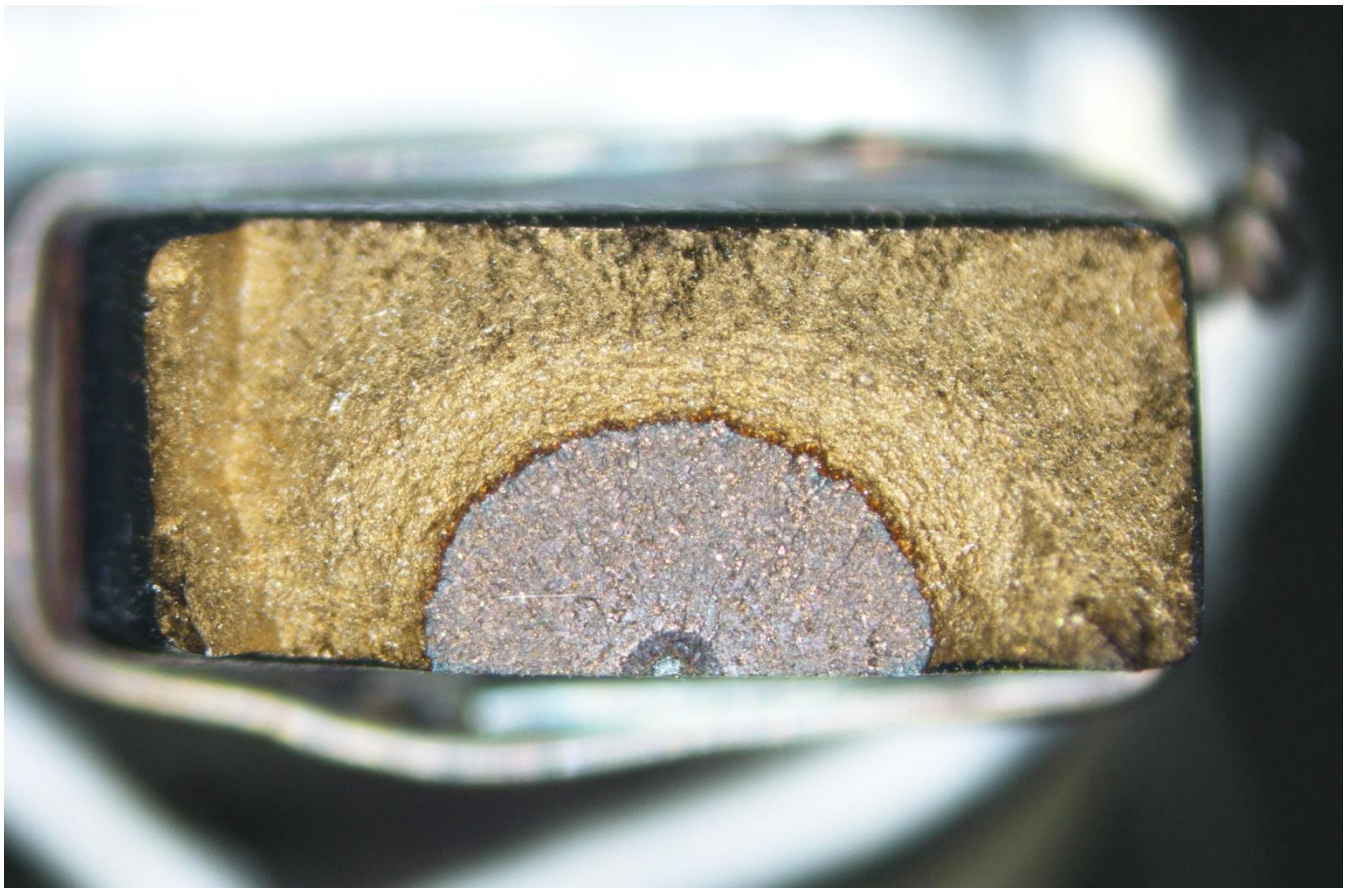

Improved data regression methods for crack growth characterization

Master's thesis in Applied Mechanics

NIKLAS AXELSSON AND JURE BARIC

Department of Applied Mechanics
CHALMERS UNIVERSITY OF TECHNOLOGY
Gothenburg, Sweden 2016

MASTER'S THESIS IN APPLIED MECHANICS

Improved data regression methods for crack growth characterization

NIKLAS AXELSSON AND JURE BARIC

Department of Applied Mechanics
Division of Dynamics
CHALMERS UNIVERSITY OF TECHNOLOGY
Gothenburg, Sweden 2016

Improved data regression methods for crack growth characterization
NIKLAS AXELSSON AND JURE BARIC

Master's Thesis 2016:18
ISSN 1652-8557
Department of Applied Mechanics
Division of Dynamics
Chalmers University of Technology
SE-412 96 Gothenburg
Sweden
Telephone: + 46 (0)31-772 1000

Cover:
Fracture surface of a test specimen of forged Inconel 718 after being subjected to cyclic loading. Three crack areas are visible; the notch, the pre-crack and the final crack area.

Chalmers Reproservice / Department of Applied Mechanics
Göteborg, Sweden 2016-07-21

Improved data regression methods for crack growth characterization
Master's thesis in Applied Mechanics
NIKLAS AXELSSON AND JURE BARIC
Department of Applied Mechanics
Division of Dynamics
Chalmers University of Technology

Abstract

The currently used method for evaluation of crack propagation in materials at GKN Aerospace Engine Systems is based on a linear relation between Potential Drop (PD) signals, registered by the testing equipment, and crack depth and width. This linear method has been proven in this report to underestimate both the crack depth and width. Other testing facilities supplying data from crack propagation tests to GKN use different methods for evaluating the crack size. The arrangements of the testing procedure and the set-up of the material specimens also differ among the parties. This leads to the issue of determining who evaluates the crack size most accurately, and how the currently used linear method can be improved.

By using test specimens with more data available for each specimen, so called calibration specimens, a different method to express crack size as a function of the PD-signals was created. This method, called Calibration Curve Adjustment (CCA) is based on an adjustable calibration curve. The calibration curve (CC) is adjusted to fit the measured crack sizes (optically evaluated after fracture), at start and end of crack propagation. The CCA approach was compared with the linear method by investigating crack sizes predicted by the two different methods and then comparing the different predictions with measured crack sizes in the calibration samples.

The CCA method was also compared with the linear method by comparing the so-called scatter factors obtained using NASGRO, a fracture mechanics and fatigue crack growth analysis software. The scatter factor indicates how well the fatigue life can be predicted according to NASGRO.

The results indicate that by using the CCA method, the crack size evolution can be more accurately predicted than by using the linear method. All tests were performed with the alloys Titanium 6Al-4V (Ti 6-4) and Inconel 718 (IN718) loaded in cyclic tension and compression with varying *R*-ratios. The CCA method gave an improved prediction for both forged Ti 6-4 and IN718 specimens. In addition, it was shown to improve predictions also for a specimen made of Ti 6-4 manufactured by additive manufacturing (AM). However, despite more accurate predictions of crack sizes, a set of 25 forged specimens made of Ti 6-4 evaluated by the CCA method did not provide a better scatter factor, as defined by NASGRO. A larger sample size (preferably 48 specimens) would however be needed to provide results with higher quality.

Key words: Potential drop, fatigue crack growth, Kb-specimen, material testing, data regression methods, Paris law, Titanium 6-4, Inconel 718, calibration curve

Contents

Preface

The work presented in this thesis has been carried out under the Division of Dynamics, Department of Applied Mechanics at Chalmers University of Technology, Gothenburg, and at GKN Aerospace Engine Systems, Trollhättan. This study has been carried out with Professor Anders Ekberg as supervisor and examiner at Chalmers University of Technology and Dr. Thomas Hansson as supervisor at GKN Aerospace Engine Systems.

We would especially like to thank Dr. Thomas Hansson at GKN Aerospace Engine Systems and Professor Anders Ekberg at Chalmers University of Technology for their guidance and support throughout the work. We would also like to thank Peter Karlsson, David Filipiak, Peter Georgsson and Dr. Tomas Månsson at GKN Aerospace Engine Systems for valuable discussions and support. Finally, for showing and explaining the procedure of crack propagation testing in the laboratory, we would also like to thank Håkan Backström and Mats Persson at GKN Aerospace Engine Systems. Their assistance has given greater understanding of the methodology used.

Göteborg 2016-07-21

NIKLAS AXELSSON AND JURE BARIC

Notations and nomenclature

Roman upper case letters

A_c	[mm^2]	Crack area.
AM		Additive manufacturing.
C	$\left[\frac{\mathrm{mm/cycle}}{(\mathrm{MPa}\sqrt{\mathrm{m}})^m}\right]$	Material parameter in Paris law.
CC		Calibration curve.
CCA		Calibration curve adjustment.
$\mathrm{CCA}_\mathrm{GKN}$		Calibration curve adjustment using calibration curve based on GKN test specimens.
$\mathrm{CCA}_\mathrm{Lab\ A}$		Calibration curve adjustment using calibration curve based on test specimens from Lab A.
DC		Direct current.
DCPD		Direct current potential drop.
F	[-]	Geometry factor of test specimen.
GKN		Guest, Keen and Nettlefolds.
K	[$\mathrm{MPa}\sqrt{\mathrm{m}}$]	Stress intensity factor.
K_max	[$\mathrm{MPa}\sqrt{\mathrm{m}}$]	Maximum stress intensity factor.
K_min	[$\mathrm{MPa}\sqrt{\mathrm{m}}$]	Minimum stress intensity factor.
L_meas	[mm]	Distance between measuring wires on the test specimen.
L_ref	[mm]	Distance between reference wires on the test specimen.
N	[-]	Number of load cycles.
PD	[-]	Potential drop value, defined as $\mathrm{PD}_\mathrm{meas}/\mathrm{PD}_\mathrm{ref}$.
$\mathrm{PD}_\mathrm{meas}$	[mV]	Potential drop value measured over the crack.
PD_ref	[mV]	Potential drop value measured over an area of the specimen unaffected by the crack.
R	[-]	Stress ratio, defined as $S_\mathrm{min}/S_\mathrm{max}$.
S	[MPa]	Nominal stress.
S_max	[MPa]	Maximum nominal stress.
S_min	[MPa]	Minimum nominal stress.
T	[mm]	Test specimen thickness.
W	[mm]	Test specimen width.

Roman lower case letters

a	[mm]	Crack depth.
a_f	[mm]	Final crack depth.
a_min	[mm]	Minimal crack depth unaffected by the notch.
a_n	[mm]	Depth of notch in test specimen.
a_s	[mm]	Crack depth at start of the test.
b_n	[mm]	Width of notch in test specimen.
c	[mm]	Half crack width.
c_1	[mm]	Semi-width of the crack measured from the centerline in one direction.
$c_{1,\mathrm{f}}$	[mm]	Final crack width in the c_1 direction.
$c_{1,\mathrm{s}}$	[mm]	Semi-width of the crack in the c_1 direction, at the start of the test.
c_2	[mm]	Semi-width of the crack measured from the centerline in the opposite direction of c_1.

$c_{2,\mathrm{f}}$	[mm]	Final crack width in the c_2 direction.
$c_{2,\mathrm{s}}$	[mm]	Semi-width of the crack in the c_2 direction, at the start of the test.
$\mathrm{d}a/\mathrm{d}N$	[mm/cycle]	Crack growth per load cycle.
m	[-]	Material parameter in Paris law.
r	[mm]	Crack radius.

Greek upper case letters

ΔK	[MPa$\sqrt{\mathrm{m}}$]	Stress intensity range, defined as $K_{\max} - K_{\min}$.
ΔS	[MPa]	Stress range, defined as $S_{\max} - \mathrm{S}_{\min}$.
Δa	[mm]	Distance from maximum notch depth to $a_{\min}$

1 Introduction

The objective of this master thesis is to improve a method currently used to evaluate crack propagation in test specimens. A more accurate method would lead to a better prediction of life for engine components within the aircraft industry. Inspection intervals for crack detection could be better planned, improving the efficiency of maintenance.

1.1 Background

Extensive mechanical testing to evaluate crack growth is common in the mechanical industry. For measurement and characterization of crack growth, the direct current potential drop (DCPD) technique is often used. This technique requires that a constant direct current is applied through the specimen. As the crack grows, the potential drop (PD) increases. The correlation between the increasing PD-signal and the growing crack is then fitted towards a predetermined relation.

The current thesis focuses on how this procedure is handled at GKN. In particular GKN collaborates with two other suppliers of mechanical testing. These suppliers also use the DCPD technique, but the procedure to evaluate the crack growth differs among the parties. The main difference is in how the PD values are measured and evaluated. This causes the same raw test data to result in different crack growth predictions depending on who carries out the evaluation.

The evolving size of the crack (as evaluated using the PD-signal) is generally used to create a graph in which the crack depth a and the crack semi-width c are plotted as a function of the number of load cycles N. Constant amplitude cyclic loads are applied to the specimen, R-value and temperature are kept constant. The recorded raw test data contains noise that needs to be removed. A filtering procedure is therefore used to ensure that the crack size is strictly increasing with increasing number of load cycles N.

When results from several specimens have been evaluated (typically twelve specimens are used for each specific temperature, four for each R-value and three R-values per temperature) a curve is fitted to the merged data and plotted in a $\mathrm{d}a/\mathrm{d}N$ versus ΔK graph. There is a difference in the number of data points belonging to each specific specimen. This causes specimens with many data points to have more impact than the specimens with fewer data points when the linear equation is fitted to all data points in a least-squares sense. It would here be beneficial to be able to assign an appropriate weight to the different data points belonging to each specimen. By doing so, each specimen gets an equal weight in the formation of the linear part of the $\mathrm{d}a/\mathrm{d}N$ versus ΔK graph.

After $\mathrm{d}a/\mathrm{d}N$ versus ΔK graphs are established along with the behavior close to threshold and fracture, the fracture mechanics and fatigue crack growth analysis software NASGRO is employed. The actual life, for each and every specimen for three R-values and several temperatures, is then compared to the crack growth life predicted by the NASGRO equation. The principal procedure behind evaluation of crack growth from tests and using NASGRO is summarized in Figure 1.1 below.

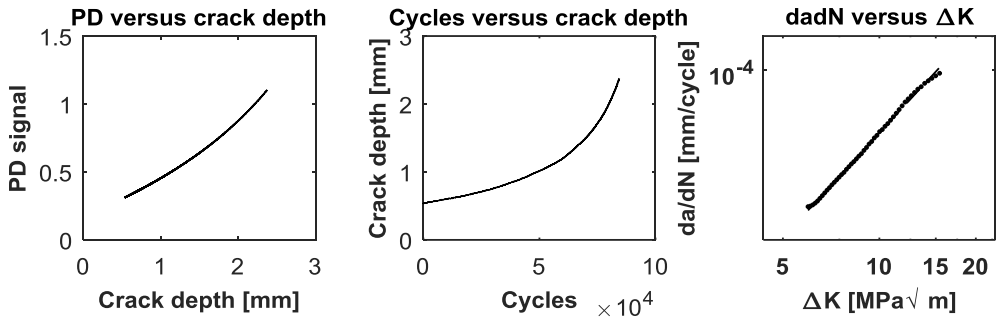

Figure 1.1. Steps in the process of evaluating crack propagation.

For each test specimen, the actual life (A) is divided by the predicted life (P). The results for specimens of a certain material can be compiled in a so-called A/P plot, as seen in Figure 1.2 below. The A/P plot is used to estimate the accuracy of the prediction model describing the crack growth. The fitted A/P value at 50 percent is divided by A/P value at 0.1 percent giving a so called scatter factor. A scatter factor closer to 1 indicates a higher accuracy of the model, i.e. the predicted life being closer to the actual life, while a higher scatter factor indicates less accuracy.

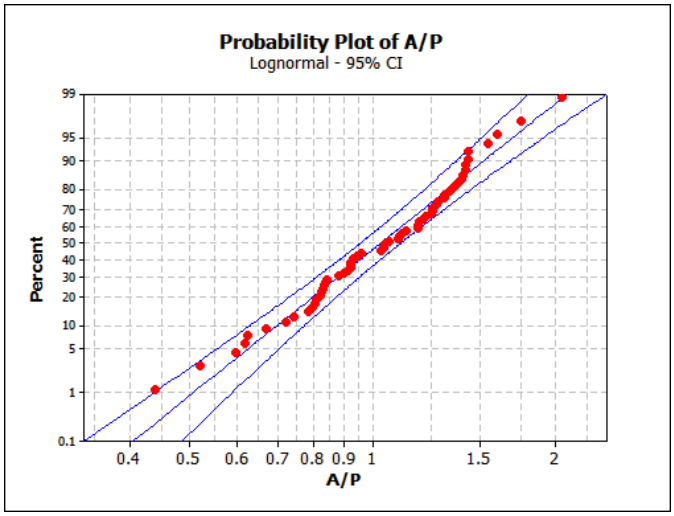

Figure 1.2. Example of an A/P plot, showing actual values over predicted values (red dots) as a function of probability. 95% confidence bounds are indicated as the outer blue lines, with a linear fit of the data shown as the line in between.

1.2 Objective

The implications and the consequences of the assumption that there is a simple linear relation between the PD-signal and the crack propagation need to be examined. This assumption may lead to an overestimation of crack growth and thereby oversized engine parts, alternatively the crack growth could be underestimated, resulting in lower safety margins than expected. The aim is to develop an alternative method that describes the relation between the PD-signal and the crack size more accurately. The purpose is to better predict the number of applied load cycles *N* that result in a certain crack size.

Furthermore, the influence of the size of the initial notch used to initiate crack growth, needs to be evaluated, as it may affect the PD-signal. The relation between crack depth a and crack width c will also be investigated to establish typical variations and provide insights in how crack propagation may be affected.

The difference between test data analysis used by GKN and other companies will be assessed. Pros and cons of the different methods will be identified. The methodology used by GKN for filtering noise will be investigated and possibly improved, e.g. by elimination of outliers in the data set. The resulting methodology should provide improved crack growth predictions from given PD-signals.

1.3 Scope

The study is primarily focused on evaluation of forged Titanium 6Al-4V (Ti 6-4) and Inconel 718 (IN718). These materials are commonly used in the aerospace industry. The test specimens are of a specific geometry type, called Kb, and loaded uniaxially with different *R*-ratios. This loading results in pure Mode I crack growth and eventually fracture. Focus is on the linear part of the $\mathrm{d}a/\mathrm{d}N$ versus ΔK curve. Conditions close to crack growth threshold as well as unstable crack growth close to fracture are included in the NASGRO analysis but is not studied in detail in this work.

2 Theory

In this chapter the instrumentation of test specimens used for crack propagation tests is reviewed. The potential drop method is briefly explained and the type of specimen used is described. The procedure of measuring the crack size is explained together with the currently used method to evaluate the crack size as a function of the PD-signal. Brief general theory and nomenclature on crack propagation is presented together with an outline of the mathematical theory of regression analysis.

2.1 Electrical discharge machining

To initiate crack growth, a notch is created on the surface of the test specimen by the use of electrical discharge machining (EDM). The spark created by EDM erodes the metal whereby material is removed, see Figure 2.1 below. This process can result in three new layers close to the notch where the material properties of the test specimen have been affected (SME 2016). On the surface layer of the specimen near the notch, spherical pieces of removed metal and electrode particles are welded to the specimen as a result of the spark. The second layer, which is also called the recast layer, can be found below the surface layer where the EDM process has changed the microstructure of the specimen. A third heat affected layer can occur where the specimen has been locally annealed. These different layers could have impact on the properties of the specimen close to the notch.

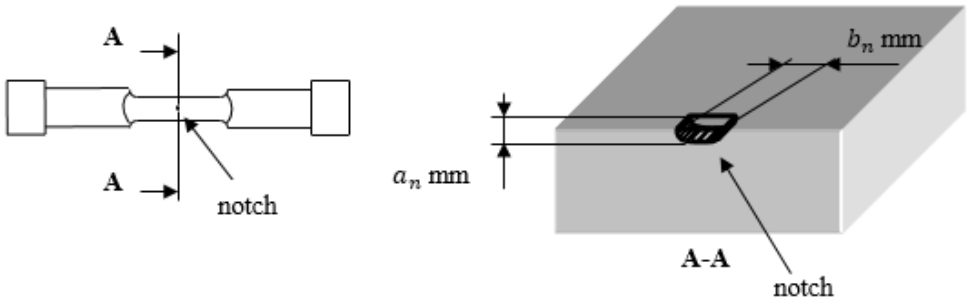

Figure 2.1. Sketch of an EDM notch on a Kb test specimen, used in studied tests. Courtesy of GKN Aerospace Engine Systems.

2.2 Direct current potential drop method

The DCPD method is commonly used for monitoring crack initiation and growth in controlled laboratory tests. At GKN a constant direct current of 10 A is applied through a Kb specimen, see Figure 2.2. There are two sets of measuring wires attached to the specimen of which one is used as reference, $\mathrm{PD_{ref}}$, and the other measures the potential drop over the crack, $\mathrm{PD_{meas}}$, see Figure 2.3 and equation (2.1) below. The reason for this procedure is to get a temperature and current independent PD-value by taking the quotient between $\mathrm{PD_{meas}}$ and $\mathrm{PD_{ref}}$.

$$\mathrm{PD} = \frac{\mathrm{PD_{meas}}}{\mathrm{PD_{ref}}} \tag{2.1}$$

As the crack grows during the fatigue test, a smaller cross sectional area of the material remains through which the current can act. This changes the resistance in the specimen and thereby the voltage through Ohm's law. An increase in voltage results in an increase in PD-signal as the measured voltage $\mathrm{PD}_{\mathrm{meas}}$ increases while $\mathrm{PD}_{\mathrm{ref}}$, which is basically unaffected by the crack, remains almost constant.

Figure 2.2. Schematic drawing of Kb specimen.

According to Gandossi et al. (2001) the translation between the PD-signal and the crack length becomes independent of material properties and thickness of the specimen through the normalized PD-signal seen in equation (2.1).

The magnitude of the PD-signal depends mainly on the distance between the measuring wires. The distances between the measuring wires, L_{meas}, and between the reference wires, L_{ref}, are detailed in Figure 2.3.

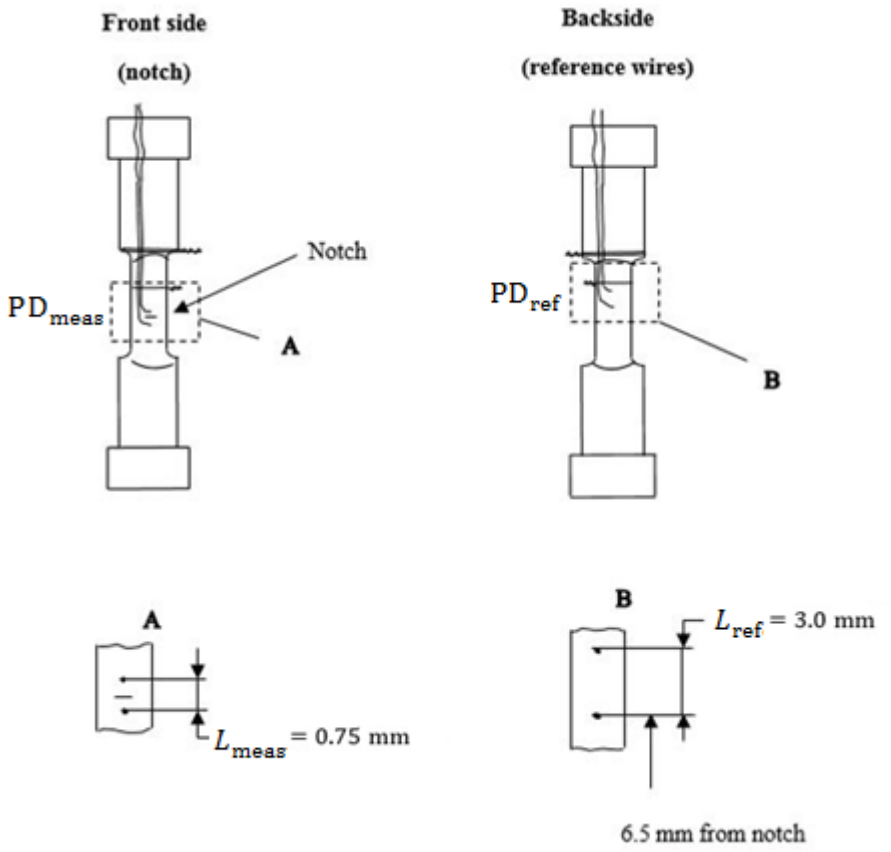

Figure 2.3. Drawing of Kb specimen with wires attached. Courtesy of GKN Aerospace Engine Systems.

According to Jensen (1999), the magnitude of the PD-signal shows a linear relation to the distance between measuring wires, L_{meas}. The symmetry of the wires in relation to the crack does not affect the PD-signal, but the distance itself has an impact on the accuracy in the prediction of crack lengths. Errors of up to ± 6 % have been predicted in FE analyses of electrical fields in the cracked specimen, depending on the value of L_{meas} and the crack size. This error may occur despite the distance of the wires being within the prescribed tolerance limits.

To ensure that the crack is not affected by the stress field in vicinity of the notch, the crack has to reach a certain depth with respect to the notch size, defined by lengths a_n and b_n according to Figure 2.1 above. ASTM (2015) prescribes equation (2.2) for determining the minimum crack depth a_{min} that fulfills this demand, see Figure 2.4 below for clarification.

$$a_{\text{min}} = a_{\text{n}} + \Delta a = a_{\text{n}} + \frac{b_{\text{n}}}{2\tan\left(\frac{15}{180}\pi\right)} \tag{2.2}$$

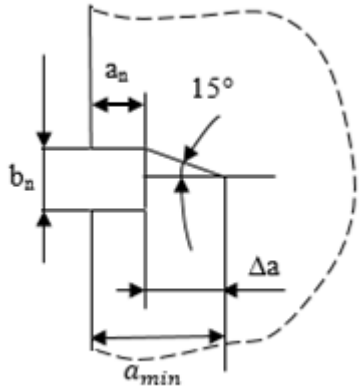

Figure 2.4. Cross-section of notched specimen showing recommended minimum crack length at the start of the test. Courtesy of GKN Aerospace Engine Systems.

The test should be terminated when the semi-width, c_f, is approximately one quarter of the specimen width W, as the used model (Newman and Raju 1981) for calculating K is valid until $c \leq W/4$, where c is the semi-width.

The Kb-specimen is heat-tinted at the start and termination of the test to enable identification of the start crack and the final crack front. A principal sketch of the crack area and the two different zones marked by the heat-tinting can be seen in Figure 2.5 below.

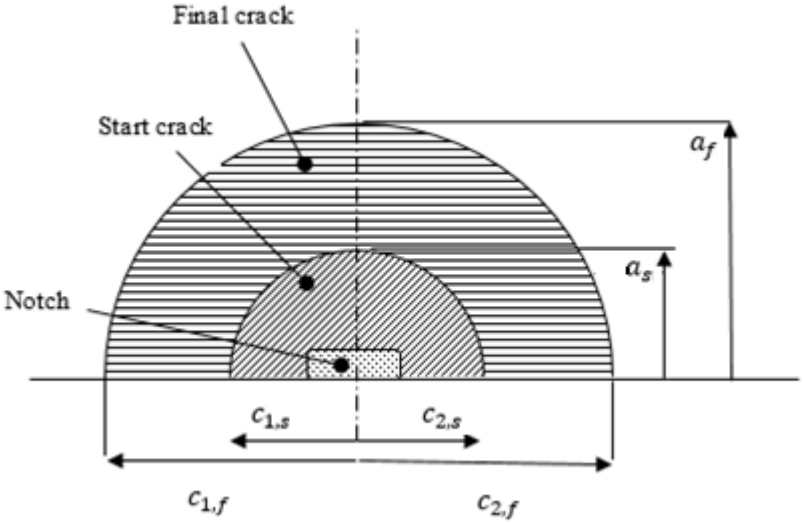

Figure 2.5. Definition of the different crack areas and lengths. Courtesy of GKN Aerospace Engine Systems.

The heat-tinting procedure leads to the formation of an oxide layer on the specimen with a certain color, as seen on the cover page. The purpose of the heat-tinting is to enable measurements of the crack sizes using optical microscopy. The heat-tinting procedure requires that the first heat-tint, which marks the crack front at the start of the test, is performed at a higher temperature than the second heat-tint (used to detect the final crack front). The reason is to avoid that the formed oxide layer from the first

heat-tint gets erased by the following tinting. The measured crack sizes are used as references to set up a curve fit of PD magnitude versus crack length, see Figure 2.6 below.

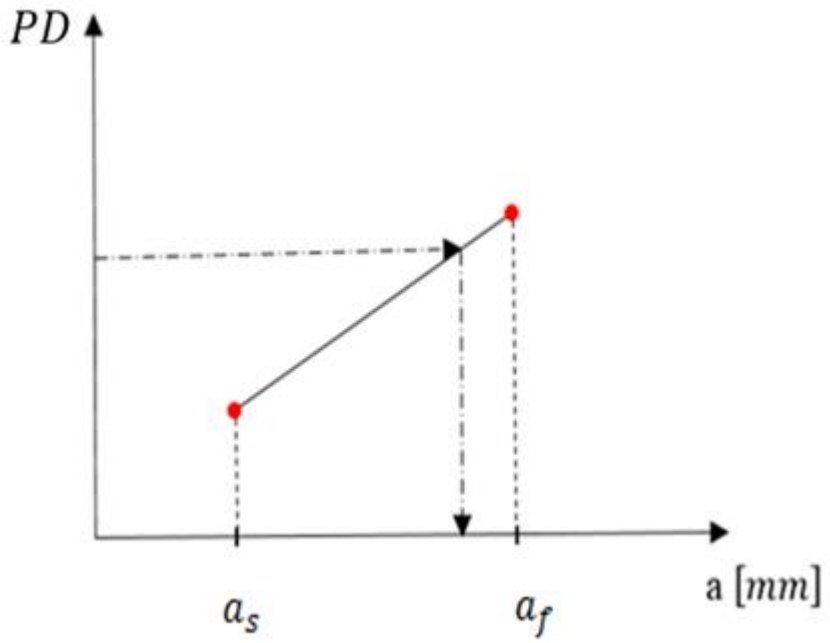

Figure 2.6. Principal sketch of usage of linear equation for determining crack size.

2.3 Fatigue crack growth

When a component is subjected to a cyclic load, small cracks are, if not already present, initiated in the material. Over time, these may grow to critical lengths and cause failure of the component. This may occur even if the applied load is well below the yield limit, see e.g. Dowling (2013).

Establishing a relation for the growth of cracks can be performed by applying a constant amplitude cyclic loading on a cracked test specimen and record the number of cycles N required to reach crack depth a (and width c). The so-called stress intensity factor (K) quantifies how severe the loading of the crack is. K depends on loading, geometry and crack size and can generally be expressed as

$$K = FS\sqrt{\pi a} \tag{2.3}$$

Where S is the applied nominal stress and F is a dimensionless geometry factor.

There are three modes in which a cracked body can be loaded and crack growth occur. These displacement modes may be combined. Pure tensional loading results in Mode I (opening mode) deformation where the crack faces move apart. Shear loading in different directions results in Mode II (sliding mode) and/or Mode III (tearing mode) deformations. See Figure 2.7 for an illustration of these modes.

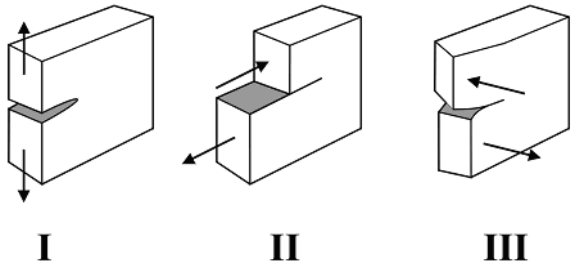

Figure 2.7. Visualization of the three displacement modes (Andrew 2016).

2.3.1 Definitions

The growth rate of a crack can be expressed as the increase in crack length (a) per cycle (N), $\mathrm{d}a/\mathrm{d}N$. To quantify the applied cyclic stress, the (nominal) stress range ΔS and the stress ratio R, are commonly used. These are defined as:

$$\Delta S = S_{\max} - S_{\min} \tag{2.4}$$

$$R = \frac{S_{\min}}{S_{\max}} \tag{2.5}$$

The crack growth rate is primarily affected by the range of the stress intensity factor, which is calculated as (cf equation (2.3)):

$$\Delta K = F\Delta S\sqrt{\pi a} \tag{2.6}$$

To account for additional influences (e.g. mid stress effects), other variables may also be accounted for (cf Dowling).

The crack growth behavior (for a specific material and temperature) is often characterized by the relation between the crack growth rate $\mathrm{d}a/\mathrm{d}N$ (defined according to equation (2.7) by Dowling (2013)) and the range of the stress intensity factor, ΔK, as plotted in a log-log scale, see Figure 2.8.

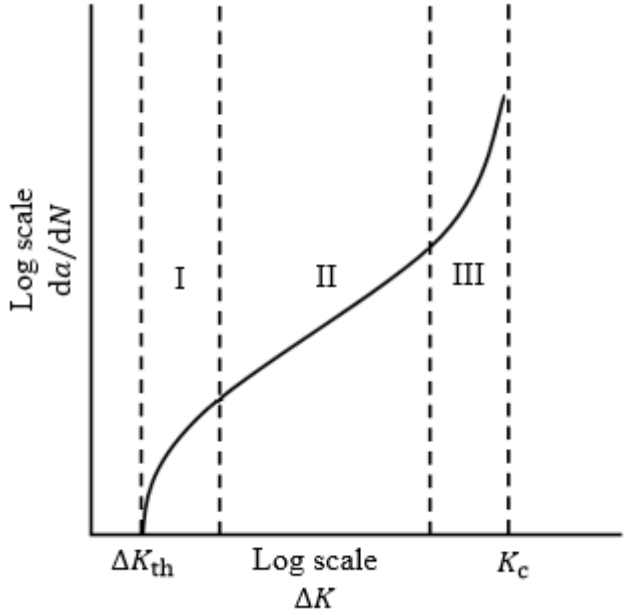

Figure 2.8. The three regions of fatigue crack growth rates.

$$\left(\frac{da}{dN}\right)_j \approx \left(\frac{\Delta a}{\Delta N}\right)_j = \frac{a_j - a_{j-1}}{N_j - N_{j-1}} \tag{2.7}$$

In region II, see Figure 2.8, this relationship can be expressed as

$$\frac{da}{dN} = C \cdot (\Delta K)^m \tag{2.8}$$

Here C and m are material parameters. The relation in equation (2.8) is commonly referred to as Paris law (Dowling 2013).

At low values of fatigue crack growth rates (region I in Figure 2.8) the crack growth curve becomes increasingly steep as it approaches a vertical asymptote. This value is called the fatigue crack growth threshold ΔK_{th} and is defined as the magnitude of ΔK below which no crack growth occurs. At very high fatigue crack growth rates (region III) the crack growth accelerates and the test specimen approaches its final failure. Here the curve approaches another vertical asymptote corresponding to $K_{\max} = K_{\text{c}}$, where K_{c} is the facture toughness of the material where (brittle) fracture occurs. For these two cases the use of ΔK and Paris law is not applicable.

2.4 Linear regression

Regression analysis is used to evaluate the relationship between one or more independent variables x_i and a single dependent variable y. In polynomial regression, the relationship is postulated as

$$y = k_0 + k_1 x_i + k_2 x_i^2 + \ldots + k_n x_i^n \tag{2.9}$$

where k are coefficients to be established, see e.g. Kleinbaum, Kupper, Muller & Nizam (1998). For data with monotonic trends, quadratic or cubic models are often sufficient to describe the data. Models of higher order than three may introduce fluctuations. Such models should only be used if there are substantial empirical or theoretical evidence to support the usage and additional verification of the model is needed.

The usage of splines can avoid these problems by providing polynomial functions that are limited to a certain range of data, transitioning into another function at the ends. Functions of order one or three are commonly used for splines. These can be established using ordinary least squares methods, as outlined in the following sections. One risk with using splines is that the functions may show very high or low values at the extreme ranges of the data set. This is because there can be a lack of data in these regions, making the function values less accurate.

When analyzing data, there can be data points that do not match the rest of the data sample for various reasons. These are called outliers and are defined by Kleinbaum et al. (1998) as any unusual or rare observation showing at the extremes of a data range, usually in y-direction. In other words, it is a data value that is much larger or smaller than the rest in that region. The occurrence of outliers may be due to extraordinary circumstances and should not be disregarded without analysis of probable origin. The presence of outliers may significantly affect the result of the fitting and should, if deemed too influential, be removed.

2.4.1 Simple linear regression

In a simple linear regression, samples of data points giving the response y are assumed to have the following linear relationship, see e.g. Adams and Essex (2010):

$$y = k_0 + k_1 x \tag{2.10}$$

Here k_0 and k_1 are unknown parameters. If the simple linear relationship is sufficiently accurate, the measured values of the response y depending on the predictor x for n data points should be approximately the same as the actual observed values and lie along a straight line. This is described in Figure 2.9 below where the circles indicate data points and vertical lines are residuals which indicate the difference between predicted and actual values. The dashed line shows the mean function, describing the average value of the function, and the full line shows the linear fit to the data.

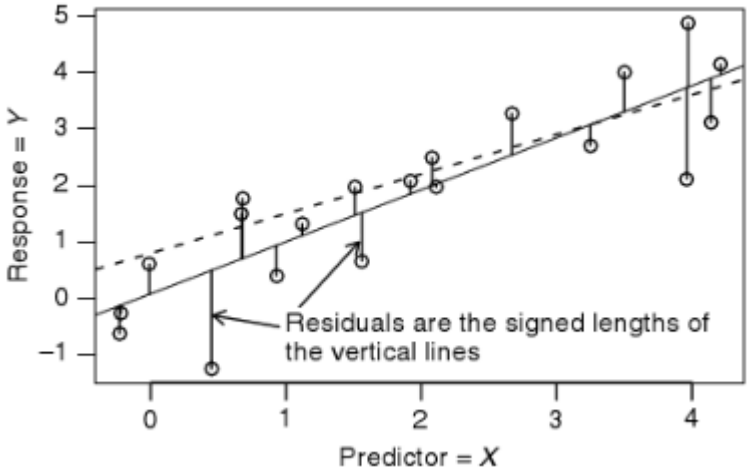

Figure 2.9. Schematic plot for fitting using ordinary least squares according to Weisberg (2013).

The objective of the linear regression is, in other words, to find the values of the parameters k_0 and k_1 so that the line in equation (2.10) most accurately fits the data. By using the method of ordinary least squares the parameters k_0 and k_1 can be chosen to minimize the sum of squares SSE of the residuals:

$$SSE = \sum_{i=1}^{n}(y_i - k_1 x_i - k_0)^2 \tag{2.11}$$

The minimum of the two parameters are found at a critical point of *S* that satisfies

$$0 = \frac{\delta S}{\delta k_1} = -2\sum_{i=1}^{n} x_i(y_i - k_1 x_i - k_0) \tag{2.12}$$

$$0 = \frac{\delta S}{\delta k_0} = -2\sum_{i=1}^{n}(y_i - k_1 x_i - k_0) \tag{2.13}$$

Equation (2.12) and (2.13) can be rewritten as:

$$(\sum_{i=1}^{n} x_i^2)k_1 + (\sum_{i=1}^{n} x_i)k_0 = \sum_{i=1}^{n} x_i y_i \tag{2.14}$$

$$(\sum_{i=1}^{n} x_i)k_1 + nk_0 = \sum_{i=1}^{n} y_i \tag{2.15}$$

Solving equations (2.14) and (2.15) above, the parameters are obtained as:

$$k_1 = \frac{n(\sum_{i=1}^{n} x_i y_i) - (\sum_{i=1}^{n} x_i)(\sum_{i=1}^{n} y_i)}{n(\sum_{i=1}^{n} x_i^2) - (\sum_{i=1}^{n} x_i)} \tag{2.16}$$

$$k_0 = \frac{(\sum_{i=1}^{n} x_i^2)(\sum_{i=1}^{n} y_i) - (\sum_{i=1}^{n} x_i)(\sum_{i=1}^{n} x_i y_i)}{n(\sum_{i=1}^{n} x_i^2) - (\sum_{i=1}^{n} x_i)} \tag{2.17}$$

2.4.2 Polynomial regression

The same procedure as described in previous chapter can be applied for a second or third degree polynomial as well, where the number of parameters increase to three and four, respectively. Performing a regression using these polynomials is described in Weisberg (2013) as quadratic and cubic regression, see equation (2.18) and (2.19) below, respectively.

$$y = k_0 + k_1 x + k_2 x^2 \tag{2.18}$$
$$y = k_0 + k_1 x + k_2 x^2 + k_3 x^3 \tag{2.19}$$

The polynomial regression model can be expressed in matrix form (MathWorks 2016), as seen in a general form in equation (2.20), in terms of response vector $\boldsymbol{y}$, design matrix $\boldsymbol{X}$, and parameter vector $\boldsymbol{k}$.

$$\boldsymbol{y} = \boldsymbol{X}\boldsymbol{k} = \begin{bmatrix} y_1 \\ y_2 \\ y_3 \\ \vdots \\ y_n \end{bmatrix} = \begin{bmatrix} 1 & x_1 & x_1^2 & \cdots & x_1^m \\ 1 & x_2 & x_2^2 & \cdots & x_2^m \\ 1 & x_3 & x_3^2 & \cdots & x_3^m \\ \vdots & \vdots & \vdots & \ddots & \vdots \\ 1 & x_n & x_n^2 & \cdots & x_n^m \end{bmatrix} \begin{bmatrix} k_0 \\ k_1 \\ k_2 \\ \vdots \\ k_n \end{bmatrix} \tag{2.20}$$

Using ordinary least squares to solve equation (2.20) gives an estimation of the parameters according to equation (2.21).

$$\boldsymbol{k} = (\boldsymbol{X}^T\boldsymbol{X})^{-1}\boldsymbol{X}^T\boldsymbol{y} = \begin{bmatrix} k_0 \\ k_1 \\ k_2 \\ \vdots \\ k_n \end{bmatrix} \tag{2.21}$$

Using quadratic or cubic regression gives the possibility to better fit general data compared with linear regression, but there are possible issues. Using polynomial functions runs the risk of giving nonsensical predictions for values which are outside of the observed data range used to fit the model. Also, as polynomials of a higher order are oscillatory and unbounded functions, sometimes a higher degree may provide a poorer fit to the data (MathWorks 2016). A lower order may also provide better predictions as it sometimes gives smoother variations between data points, and thus may be more suitable for monotonic data.

2.4.3 Evaluation of regression analyses

Minitab (2016a) describes the Anderson-Darling (AD) statistic as a measurement of how well a set of data follows a specified distribution. The so called p-value, or p-statistic, is used to determine if results of an analysis is statistically significant, according to Minitab (2016b). It can also be described as an indication if the analyzed data comes from the chosen distribution.

Weisberg (2013) describe fitted values and estimates of regression coefficients to all be subjected to a degree of uncertainty. Kleinbaum et al (1998) describe that confidence intervals show how certain it is that the estimates are within an interval.

2.5 Crack growth testing using PD measurements

Gandossi et al. (2001) describes advantages and disadvantages of using DCPD and examines the accuracy of using calibration curves to predict crack growth. In this case, the calibration curves have been obtained by 2D- and 3D FE analysis of test specimens. The DCPD method is used as it (according to Gandossi et al. (2001)) has

many advantages – it is flexible, has a simple instrumentation and enables continuous monitoring of the crack while not requiring visual access to the specimen. Also, very small increments can be detected and it is robust and suitable for automation. The drawbacks are also described – the method requires a calibration curve (or an alternative way of interpreting the PD-signal) and there is a risk of underestimation of the crack size, should the two crack faces come into contact.

Gandossi et al. (2001) also states that by using a normalized voltage, $PD_{\mathrm{meas}}/PD_{\mathrm{ref}}$ versus normalized crack depth, a/W, the calibration curves become independent of material properties, test specimen thickness and the magnitude of the current applied on the specimen. The calibration curves are basically functions of the geometry of specimen and crack and the locations of current input and potential measurement wires.

Calibration curves can be derived analytically, numerically or empirically based on some key assumptions, e.g. that material properties changes in temperature and strain are considered to have negligible effect on the calibration curve (Tarnowski, Davies, Nikbin and Dean (2014)). Even though these assumptions may not be completely true, the factors which influence the specimen (e.g. temperature variations, thermal ageing and global strain) can be minimized through the normalization of the PD using a reference measurement taken at a distance from the crack.

Georgsson (2000) identifies and evaluates possible uncertainties regarding crack length measurement and crack propagation rate when using the DCPD method for a typical superalloy. Kb-specimens with a crack size of 0.25—2.5 mm at room temperature are tested according to the ASTM E647 and E740 standards. The test specimens evaluated are subjected to uniaxial loading with constant load amplitude and have uniform gauge lengths. Typical sources of uncertainty are given together with their probable contribution to fatigue crack growth parameters, such as crack length, stress intensity factor and crack growth. The sources of the uncertainties include the test piece geometry, test system, environment and test procedure. Each source of uncertainty is estimated to either have a major, minor or no contribution to the crack growth parameters. It is also shown how the uncertainties are calculated and accounted for in the parameters.

Jensen (1999) examined how the position of the measuring and the reference wires affected the magnitude of the PD-signals. This was done by FE analysis of the electrical fields in the material specimens where the effect of crack length on the PD-signal magnitude was investigated. The conclusion reached by Jensen was that the impact of the placement between the measuring wires on the PD-signals decreases linearly as the crack grows. The placement of the measuring wires has a stronger impact for short cracks. Both the measuring and reference wires were found to be more affected by the absolute distance between the wires rather than the symmetry with respect to the center of the crack.

3 Method and analysis

The current thesis examines crack propagation in Kb-specimens. Data from crack propagation tests have been used to establish a mathematical model for crack growth. Calibration specimens, for which more (fractographically obtained) crack length versus PD data are available for each specimen, were used to establish a calibration curve to describe the translation between PD and crack dimension. This general CC is adjusted to match a_s and a_f for each tested Kb-specimen. The developed method is compared to the linear method of describing crack growth behavior through tests of Kb-specimens containing one or more crack length versus PD data points between a_s and a_f. Predicted crack sizes according to the two different methods for the corresponding PD-signals were compared with the optically measured crack sizes.

Other possible improvements to the currently used method through improved filtering of noise were examined. These included removal of outliers in the crack length versus load cycle data, and alternative filtering techniques. The goal is here to increase the quality of the input data. The impact of the possible improvements is studied by comparing actual fatigue life with numerically predicted fatigue life, using NASGRO. All data used in the examination and testing of the methods were provided by GKN Aerospace.

3.1 Crack geometry

The data from the calibration specimens, together with visual post fracture inspections of Kb-specimens, were used to examine the relation between crack growth in a and c directions (as detailed in Figure 3.1). The size of the notch in the specimen and how (or if) it affects test data was examined by evaluating different Kb-specimens with smaller and larger notch sizes.

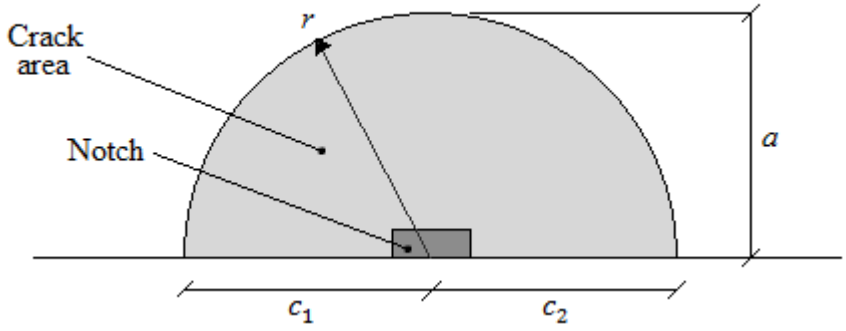

Figure 3.1. Cross section of crack area with defined directions and the notch indicated.

3.1.1 Crack shape

The area of the presumed semi-circular crack when assumed to be half-circular was estimated as:

$$A_c = \frac{r^2\pi}{2} \tag{3.1}$$

Where r is the average crack depth, defined in Figure 3.1, measured at angles from 0° to 180° in steps of 45°. The area of a presumed semi-elliptical crack was estimated as:

$$A_c = \frac{\pi ac}{2} \tag{3.2}$$

Where a is the crack depth and c is the semi-width of the crack. Since the semi-widths c may not be the same in the left and right directions, a more accurate representation of the crack area would be to consider the crack area as two quarter-ellipses and estimate the area as:

$$A_c = \frac{\pi ac_1}{4} + \frac{\pi ac_2}{4} = \frac{\pi a}{4}(c_1 + c_2) \tag{3.3}$$

The examination of the crack growth in a and c direction of the calibration specimens, together with the inspection of crack shape geometry of Kb-specimens post fracture, is pointing towards a semi-elliptical crack shape. A semi-elliptical crack growth is supported by ASTM International (2004), which claims that the crack is expected propagate faster in the c direction than in the a direction, see Figure 3.2.

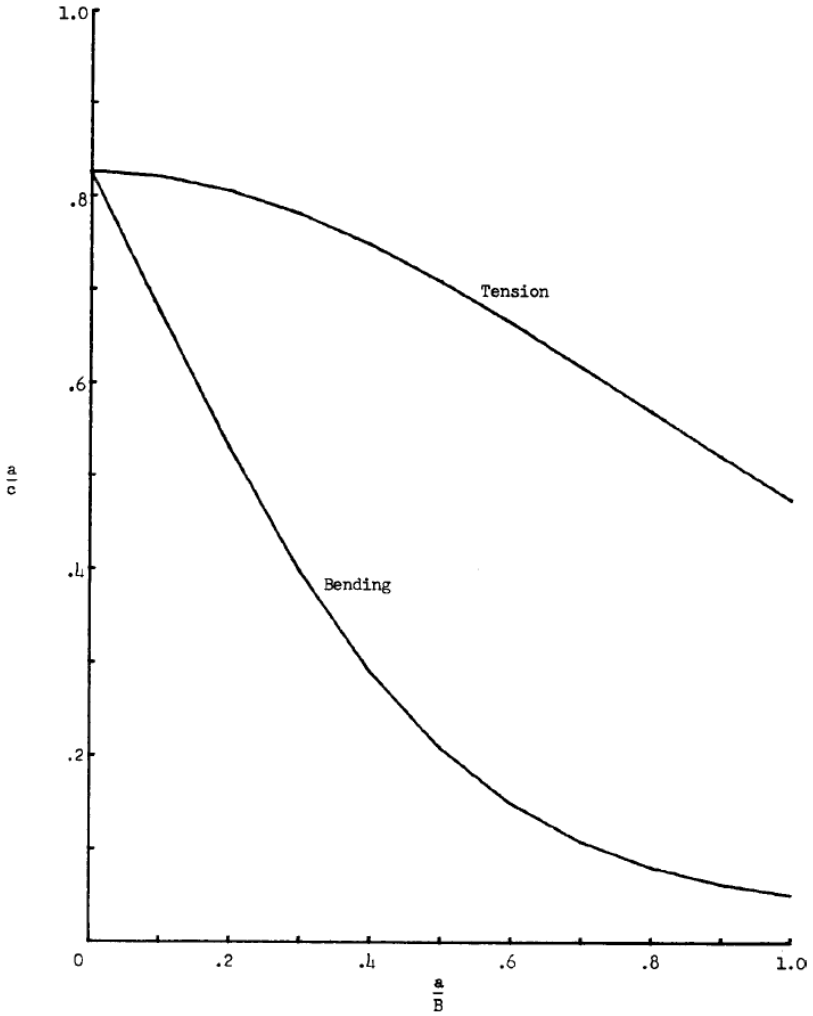

Figure 3.2. Relation between crack depth a and width c for a specimen of breadth B, loaded in tension and bending (ASTM International 2004).

3.2 Predicting crack size

In order to evaluate the relation between PD-signal and crack depth and width, data from calibration specimens were used. These specimens were tested using extra heat-tintings, which upon post fracture examination provides more available data that connect measured PD-signals to specific crack sizes. By merging all data from these calibration specimens for the materials Ti 6-4 and IN718 regression analysis was performed to derive a relation between crack size from a given PD-signal.

Three functions were examined. First, second and third degree polynomials with PD as a function of a, c_1, c_2 and of crack area A (evaluated using equation (3.3)). All regression analysis was performed in MATLAB using built-in functions that use a least-square method to minimize the error. Using a first degree polynomial would correspond to the currently used method. The accuracy of the created polynomial functions was examined by studying the error between predicted and measured crack depth and width for the test specimens. The alternative of expressing crack growth in terms of crack area as a function of PD-signals was also investigated. This alternative was considered to have the possibility to perhaps more accurately describe the crack

growth, as all growth directions would have been taken into account. However, through optical measurements it was found that the cracks grow in a semi-elliptical shape and often asymmetrically. The method of describing the crack using area was therefore dismissed in favor of using crack depth and width. The third degree polynomial functions proved to be the most accurate. In the improved model the calibration curves for each material are therefore based on third degree polynomial functions.

3.2.1 Calibration Curve Adjustment (CCA)

The method of using the calibration curve to predict crack size was extended and an additional process, a curve adjustment with respect to measured a_s and a_f, is carried out to adjust the curve. The difference (or correction) between the CC predicted crack start: $CC(PD_s)$ and finish: $CC(PD_f)$ is compared with the measured magnitudes of a_s and a_f. This difference was assumed to have a simple linear relation to the PD-signal, like the distance between measuring wires and the PD-signal as described by Jensen (1999). This procedure enabled an estimation of all differences for the whole sequence of PD-signals between a_s and a_f. This difference e (measured in millimeters) is calculated according to

$$e(\mathrm{PD}) = k \cdot PD + m \tag{3.4}$$

where k and m can be calculated from a comparison between measured a_s and a_f values and crack sizes predicted using the calibration curve, $CC(PD)$, for corresponding PD-signals PD_s and PD_f. This gives the differences at start: e_s and at finish: e_f, according to equation (3.5) and (3.6) below.

$$e_s = CC(PD_s) - a_s \tag{3.5}$$
$$e_f = CC(PD_f) - a_f \tag{3.6}$$

By solving equation (3.5) and (3.6) the slope, k, and the intercept m can be solved as

$$k = \frac{e_f - e_s}{\mathrm{PD}_f - \mathrm{PD}_s} \tag{3.7}$$
$$m = e_s - k \cdot \mathrm{PD}_s \tag{3.8}$$

Using the assumption of a linear relationship between the differences of measured and predicted crack sizes at start and finish according to CC, the calibration curve can then be adjusted as follows:

$$CCA(PD) = CC(PD) - e(PD) \tag{3.9}$$

The calibration curve is adjusted to match the only two data known for all test samples, namely a_s and a_f. The crack sizes of the specimen, expressed as a function of the measured PD-signals, are then adjusted with respect to the linear difference along the entire PD-interval. The process of CCA is visualized in Figure 3.3 below. Step 1 describes the initial situation where the calibration curve is unadjusted and there is a difference between the predicted and the measured crack sizes. Step 2 shows the assumed distribution of the difference over the entire range of PD-signals and step

3 displays the adjusted crack growth curve, where differences have been taken into account.

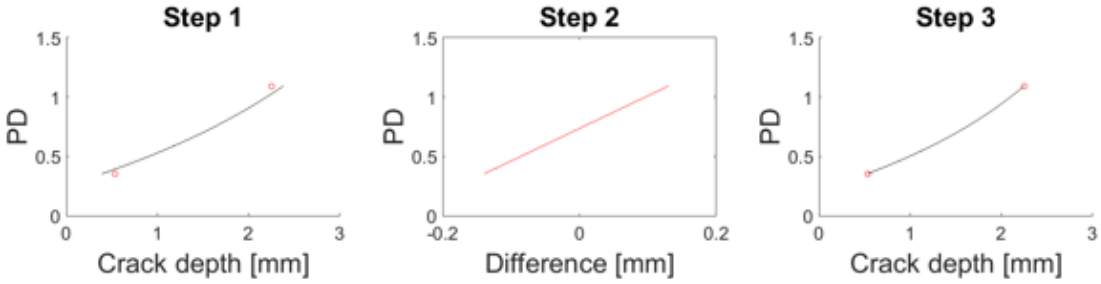

Figure 3.3. Steps in the CCA process of predicting the crack size using PD-signals.

3.2.2 Accuracy of calibration curves

To investigate the robustness with respect to material properties of the calibration curve an additional crack propagation test was run at GKN. The Kb-specimen used for this test was made of Ti 6-4 and manufactured by additive manufacturing (AM). An extra heat-tint was performed approximately half way through the crack propagation test and the corresponding PD-signal was registered. Crack sizes predicted from the registered PD-signal were compared against crack sizes optically measured in a microscope (see cross section of the Kb-specimen in Figure 3.4).

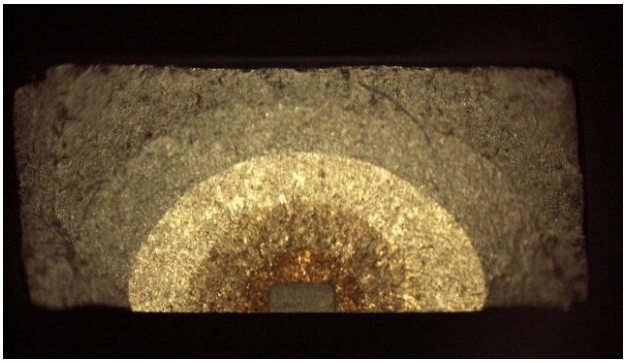

Figure 3.4. Cross section of Kb-specimen with different crack areas visible through heat-tinting. The notch area is seen as the gray rectangle at the lower edge of the specimen.

3.3 Handling data from external suppliers

In general the coupling between PD-signals and crack size (i.e. the calibration curve) depends mainly on the method used to express crack size as a function of the PD-signals, and on the testing procedure. Consider a case where two external laboratories – Lab A and Lab B – use different methods to evaluate crack propagation. The consequence of this is that the recorded PD-signals are interpreted and recorded differently between the two suppliers. Furthermore, parts of the sequence of PD-signals from crack propagation tests supplied by Lab A and Lab B may be outside the interval for which CCA_{GKN} (the calibration curve derived according to the procedures in section 3.2) is considered valid. For these reasons, pre-processing is necessary to

adjust the magnitude of the PD-signals in order to ensure that the complete sequence fits $\mathrm{CCA_{GKN}}$.

Lab B uses a similar method to the one currently used at GKN to evaluate crack propagation. One major difference is that the PD-signals coupled to the crack lengths are registered at peak load by GKN. In contrast, Lab B randomly registers PD-magnitudes five times during a number of load cycles and an average of these five PD-signals is used. The Kb-specimens are heat-tinted to enable measurement of the crack fronts in the optical microscope just as at GKN. A linear relation between the PD-signals and crack length is assumed.

Lab A uses an analytical method based on the Roe-Coffin potential drop solution (VanStone, Richardson (1985)), described in Appendix I. The cyclic loading is paused at varying intervals and heat-tints are performed. The Kb-specimens are heat-tinted to enable post-fracture measurements in the optical microscope to define start and final crack, as usual.

The procedure of how the PD-signals are handled to fit $\mathrm{CCA_{GKN}}$ is illustrated by Figure 3.5 below. A Kb-specimen supplied by Lab A is used as an example but the same procedure is applied on specimens from Lab B. In step 1, the raw test data as supplied by Lab A is plotted as a function of crack size by the mathematical function of $\mathrm{CC_{GKN}}$. The magnitude of the PD-signal according to $\mathrm{CC_{GKN}}$ that matches the measured a_s is then evaluated.

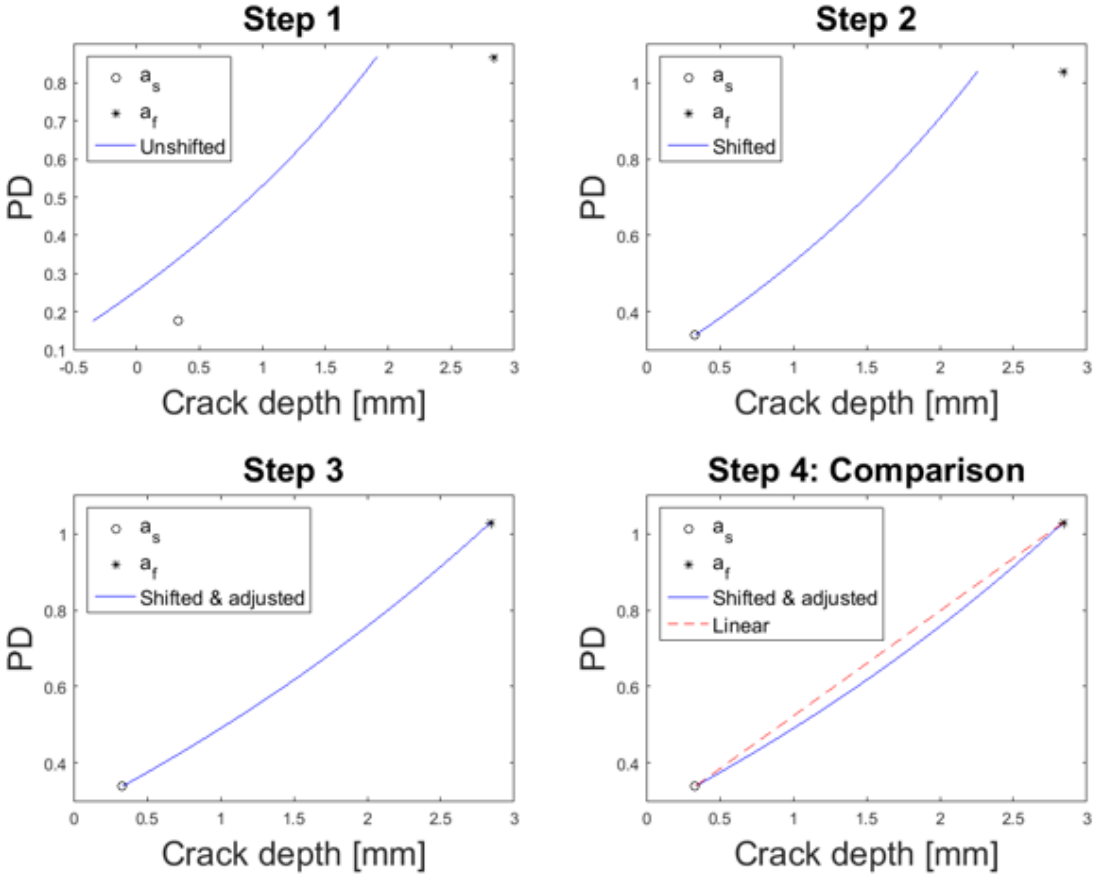

Figure 3.5. Different steps in the handling of external data visualized.

The difference between the original PD-value supplied by Lab A coupled to a_s and the PD-value according to CC_{GKN} coupled to a_s is used to shift the whole sequence of the PD-signals supplied by Lab A. The result of the shift is that CC_{GKN} matches a_s, as seen in step 2 in Figure 3.5. However, the curve terminates at a different crack depth than the measured a_f. The difference between the predicted crack depth where the curve ends and a_f is corrected by adjusting CC_{GKN} as described in section 3.2.1 and the result of this correction is that the curve matches both a_s and a_f, as seen in step 3. In step 4, the linear method (dashed red line) is compared to this new method to handle external data. In particular it may be noted that the new method predicts a longer crack for a given PD-signal.

3.4 Filtering and weighting of data

In order to achieve a robust representation of the crack growth, the crack length versus number of cycles needs to be filtered to reduce noise. The present day method creates an 11-point running average of data points and rounds off crack lengths to the nearest hundredth of a millimeter. Crack values smaller than a_{min}, according to equation (2.2), and larger than a quarter of the specimen width (typically around 2.5 mm) are deleted as these are outside the applicable range for calculating ΔK (Newman & Raju 1981).

In this current methodology, no regard is taken to weighting of data points. This means that specimens with less measured data will have a smaller impact on the formation of the da/dN versus ΔK curve, while specimens with more registered data will have a larger and more dominating impact when data from all specimens are merged.

The lack of weighting and alternatives for filtering were studied. A tool to do filtering, weighting and removal of outliers is Shape Language Modeling (SLM). SLM is a MATLAB curve fitting tool that creates a spline function of input data (D'Errico 2009). It uses hermite polynomials, a type of polynomial sequence, to express a first or third degree polynomial function created using a least-squares method. It gives control over the number of data points given as output, degree of the polynomial function used, and number of so called knots, where one function is replaced by another. Functions can also be prescribed to be constantly increasing, which is what is physically expected in crack propagation. The start and end values can be prescribed, which is used here to fix the functions at the known crack measurements.

By creating a logarithmical distribution of da/dN values with a specific number of data points, the issues of outliers and deviating data (which are currently removed manually), varying density of data for each specimen and the different amount of data in each specimen can be accounted for. This logarithmical distribution of the values is done by creating an interval of logarithmically distributed crack lengths (both a and c values) between start and final crack sizes. The number of cycles corresponding to these values are then evaluated. As there rarely is a cycle number matching the crack length exactly, an approximation is used. This requires that the number of data points created by SLM must be large (approximately 100 times larger) compared to the number of logarithmically distributed points later used.

3.5 Crack growth and stress intensity

Crack growth was evaluated using equation (2.7), which is the preferred method at GKN. The pertinent stress intensity range was numerically calculated by using the currently preferred method at GKN, called NASA TM-83200 as described by Newman and Raju (1981). This method is developed for specimens subjected to tensile loading, where the stress intensity factors can be found as functions of crack depth, crack length, parametric angle, plate thickness and width. This method is to be used for semi-elliptical surface cracks. For a detailed description of NASA TM-83200, see Appendix II.

3.6 NASGRO and A/P plots

To compare numerically predicted crack growth rates and fatigue lives to experimentally found values, the software NASGRO 6.21.2 Themelio was used. More specifically, the NASGRO program NASFLA was used for analysis of crack propagation for surface cracks. The equation used by NASGRO for calculating crack growth can be expressed as (Southwest Research Institute 2016)

$$\frac{\mathrm{d}a}{\mathrm{d}N} = C\left[\left(\frac{1-f}{1-R}\right)\Delta K\right]^n \frac{\left(1-\frac{\Delta K_{\mathrm{th}}}{\Delta K}\right)^p}{\left(1-\frac{K_{\mathrm{max}}}{K_{\mathrm{c}}}\right)^q} \tag{3.10}$$

This equation takes into account both the near-threshold value (seen as the numerator in the equation) and the near-instability regions (seen as the denominator in the equation). Remaining variables describe the linear Paris curve (mid stress corrected and with crack closure considered). Previous analyses describing the threshold, unstable crack growth and the linear Paris curve, along with material and geometrical characteristics provided all necessary data to perform full calculations using the software. This enables a prediction of crack growth for the specimens.

The data samples include testing at several temperatures. For each temperature, three R-values are used, each with ideally four specimens, making a total of 12 specimens per temperature.

A lognormal probability plot is created using data from NASGRO calculations. The actual (experimentally found) fatigue life (A) is divided by the predicted fatigue life (P) (using NASGRO) for each test specimen. This gives one A/P value for each specimen. Derived A/P values are visualized in a lognormal probability plot of all the data with 95% confidence bounds indicated, as seen in Figure 1.2. A so called scatter factor (*SF*) is calculated by dividing the A/P value at 50% with the (predicted) A/P value at 0.1%, as below.

$$SF = \frac{\left(A/P\right)_{50\%}}{\left(A/P\right)_{0.1\%}} \tag{3.11}$$

The closer the SF value is to 1, the better the overall accuracy of the model. Preferably the A/P value at 50% should be close to 1 and have a small scatter, as this indicates a more accurate prediction of the actual fatigue life.

Should the A/P value at 50% be smaller than 1 the mean curves describing the behavior of the material would be non-conservative. This is not desirable and therefore the parameter C from Paris law, described in equation (2.8), is divided by the non-conservative A/P value at 50%. The parameter C will then increase and a new A/P at 50% is calculated using the new C. This correction continues until a A/P value at 50% above 1 is found.

4 Results and discussion

Of the three testing laboratories, GKN and Lab B have similar procedures. The differences between these two lie mainly in how the PD-signals are registered and the arrangement of the measuring wires on the Kb-specimens. While GKN registers the PD-signals at extreme loads (max and min), Lab B registers several measurements for each cycle and uses the average of these.

Lab A uses an analytical solution called Roe Coffin, described by VanStone, Richardson (1985), and briefly explained in Appendix I, to model the crack growth as a function of PD-signals. The PD-signals supplied by Lab A are also of a different magnitude and do not match the interval of the calibration curve of GKN.

The distance to be kept between the measuring wires, according to protocol, is different for GKN and the other testing laboratories. This result in different magnitudes of the PD-signals, which do not match the interval of the calibration curve designed for GKN.

4.1 Coupling of PD-signals to crack size

By using the CCA method as described in section 3.2.1 the crack size is more conservatively predicted than if a linear method is employed. Figure 4.1 below illustrates the principal difference between the two methods. By following the black arrows in the figure it can be seen that for the same PD-signal different crack depths, a_{lin} and a_{CCA}, are obtained depending on which method that is being used. CCA predicts a crack depth larger than the linear method for all PD-signals between a_{s} and a_{f}.

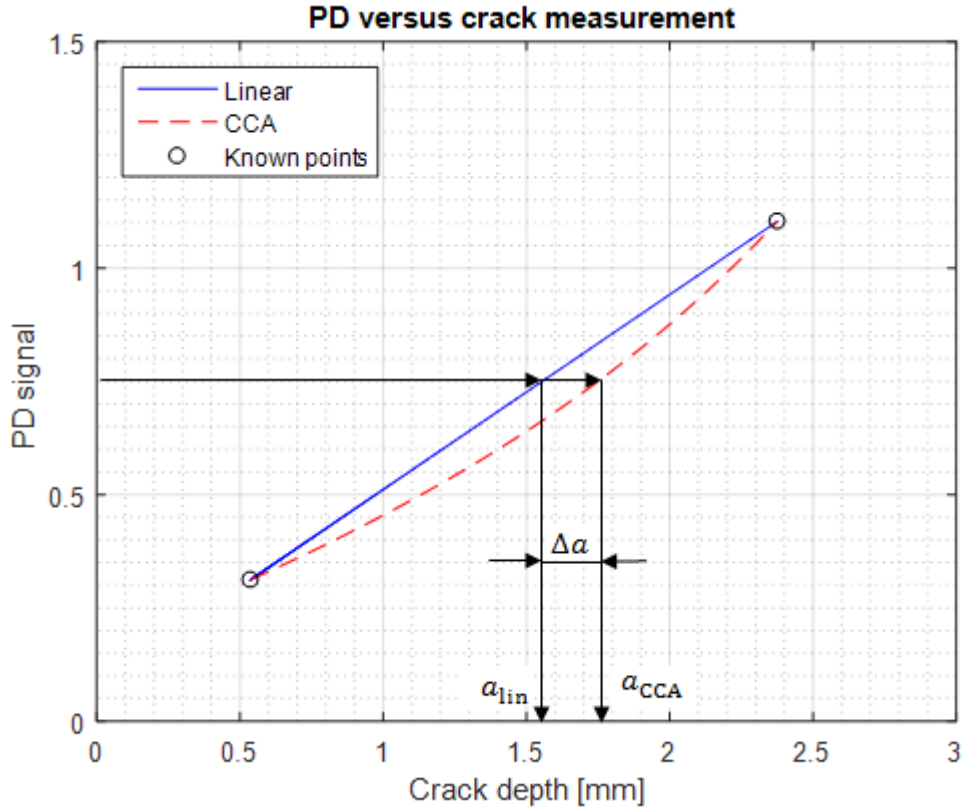

Figure 4.1. PD-signals versus predicted crack depths using linear method (a_{lin}) and the new CCA method (a_{CCA}).

4.1.1 Calibration specimens

The establishment of a calibration curve is based on a population of five Kb-specimens of Ti 6-4, each with four registered crack sizes for a, c_1 and c_2 and corresponding PD-signals. These five specimens add up to a total of 20 PD-signal magnitudes with corresponding measured crack sizes, see Figure 4.2. Similarly, a calibration curve was created for IN718 using 5 specimens and 19 PD-signal magnitudes with corresponding crack sizes, see Figure 4.3. The lowest and highest values of the PD-signal in the population are 0.336 and 1.366 for Ti 6-4 and 0.377 and 1.277 for IN718. PD-signals outside this range are translated using an extrapolated relation, and thus the accuracy to predict crack sizes decrease. This is especially the case since CCA is based on a third degree polynomial and therefore sensitive to extrapolation, as described in section 2.4.2. Consequently the currently used linear method is more robust in the sense that it can handle any PD-value without major risks of large errors, while the new CCA method is limited to a certain crack size interval.

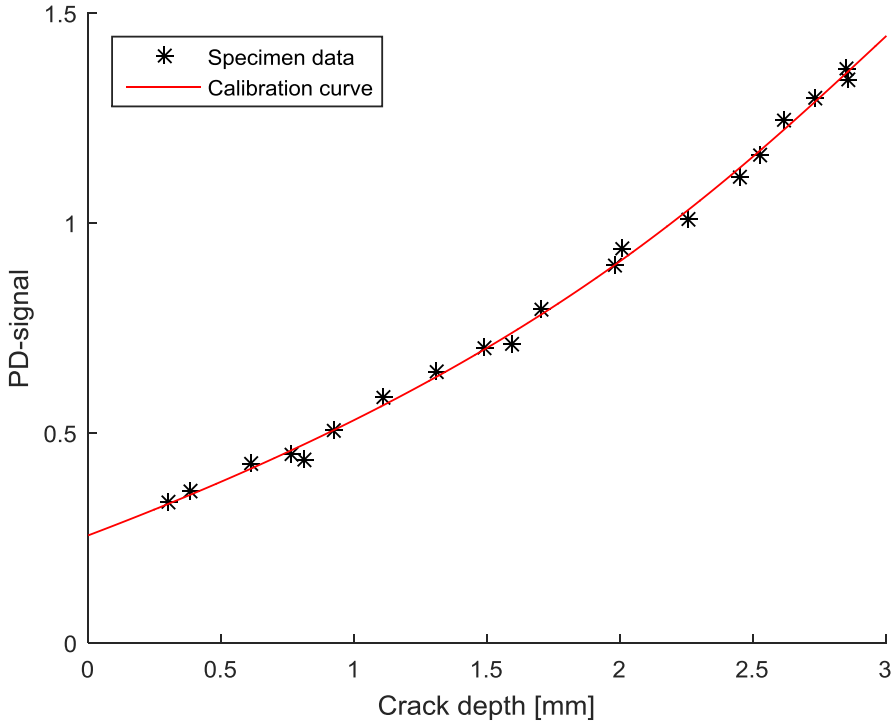

Figure 4.2. PD-signal versus crack depth for calibration specimens of forged Ti 6-4.

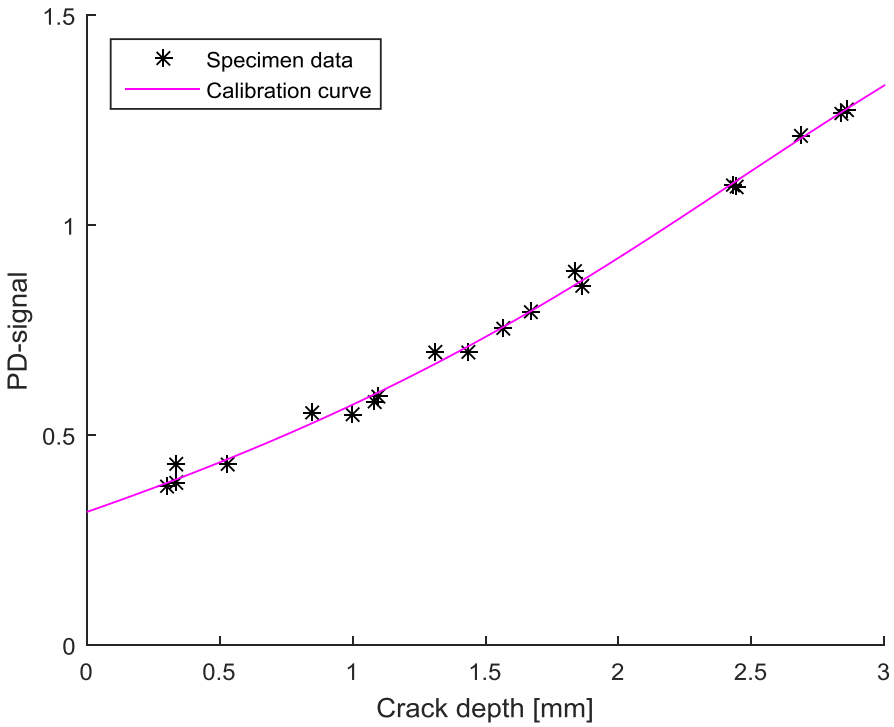

Figure 4.3. PD-signal versus crack depth for calibration specimens of forged IN718.

4.1.2 CCA compared with the linear method

The CCA method of modeling and predicting crack growth tested against the calibration specimens showed that CCA is more accurate than the linear method. The average and max differences of the two sets of calibration specimen data are presented in Table 4.1 to Table 4.4 below. The data for forged IN718 contains nine points while the data for forged Ti 6-4 contains ten points, distributed on five specimens each. A full table with the differences for all points and specimens is found in Appendix III

Table 4.1. Difference in crack size prediction of calibration specimens made of IN718 using Ti 6-4 calibration curve.

	CCA method		Linear method	
Crack direction	Average difference	Max difference	Average difference	Max difference
a	0.0278	0.0863	0.1679	0.2691
c_1	-0.0069	-0.0790	0.1063	0.1856
c_2	-0.0004	-0.0794	0.1067	0.1888

Table 4.2. Difference in crack size prediction of calibration specimens made of Ti 6-4 using Ti 6-4 calibration curve.

	CCA method		Linear method	
Crack direction	Average difference	Max difference	Average difference	Max difference
a	-0.0158	-0.0492	0.1335	0.1976
c_1	-0.0144	-0.0663	0.1030	0.2113
c_2	-0.0144	-0.0497	0.0973	0.1884

Table 4.3. Difference in crack size prediction of calibration specimens made of IN718 using IN718 calibration curve.

	CCA method		Linear method	
Crack direction	Average difference	Max difference	Average difference	Max difference
a	0.0412	0.1043	0.1679	0.2691
c_1	0.0381	0.1038	0.1063	0.1856
c_2	0.0431	0.1096	0.1067	0.1888

Table 4.4. Difference in crack size prediction of calibration specimens made of Ti 6-4 using IN718 calibration curve.

	CCA method		Linear method	
Crack direction	Average difference	Max difference	Average difference	Max difference
a	-0.0061	-0.0427	0.1335	0.1976
c_1	0.0391	0.0898	0.1030	0.2113
c_2	0.0333	0.0582	0.0973	0.1884

The fact that the calibration specimens made of Ti 6-4 evaluated by the calibration curve based on Ti 6-4 and the calibration specimens made of IN718 evaluated by the calibration curve based on IN718 were predicted with high accuracy was expected, since the calibration curves are created based on the data from the evaluated specimens. The small difference between predicted and measured values indicates that CCA is insensitive of material, provided it is IN718 or Ti 6-4. However, the tested population is too small to reach any final conclusions. In Appendix IV the difference between measured and predicted crack sizes with respect to crack size is plotted. The calibration curve based on Ti 6-4 is used to evaluate the calibration specimens made of Ti 6-4 and IN718. The calibration curve based on IN718 is also used to predict the crack sizes of the calibration specimens made of IN718 and Ti 6-4. It can be seen that the linear method always underestimates the crack size while CCA in some cases overestimates the crack size. The magnitude of the difference between measured and predicted crack size does not seem to depend on the crack size.

4.1.3 Additive manufacturing specimen

A crack propagation test for a Kb-specimen manufactured by AM was also used to compare the ability of CCA with the linear method to predict crack size. The specimen was made of Ti 6-4, the grain sizes were similar to the grain sizes of forged Kb-specimens. The evaluation showed that the CCA method predicted both crack depth and width more accurately than the linear method for this specimen as well. Table 4.5 and Table 4.6 shows measured and predicted crack sizes for the evaluated AM-specimen and the difference between predicted and measured values.

Table 4.5. Prediction of crack sizes using CCA method.

Crack direction	Measured [mm]	Predicted [mm]	Difference [mm]
a	1.9220	1.9635	-0.0415
c_1	2.0660	2.0502	0.0158
c_2	1.9720	1.9842	-0.0122

Table 4.6. Prediction of crack sizes using linear method.

Crack direction	Measured [mm]	Predicted [mm]	Difference [mm]
a	1.9220	1.8079	0.1141
c_1	2.0660	1.9397	0.1263
c_2	1.9720	1.8766	0.0954

Using CCA, a and c_2 are slightly overestimated while c_1 is slightly underestimated. CCA was in all cases able to predict the crack size more accurately than the linear method which underestimated the crack size in all three directions, resulting in an overestimation of predicted safety margins in operational use. To draw more definitive conclusions on the applicability of CCA on AM-specimens further crack propagation tests are however needed.

The AM-specimen also presented an opportunity to examine the impact of the notch size. The specimen had a notch width b_{n} of almost 1.2 mm while the other Ti 6-4 specimens from GKN had notch widths b_{n} as small as 0.3 mm. Based on the

difference between the predicted and measured values, without any adjustment of the calibration curve, there was an underestimation of the crack sizes for the AM-specimen, as seen in Figure 4.4 below. The cause of the underestimation may be due to the larger notch, but since CCA provided accurate predictions and did not show any largely deviating behavior, the tentative conclusion is that the size of the notch does not seem to have a major influence on CCA based prediction of crack size.

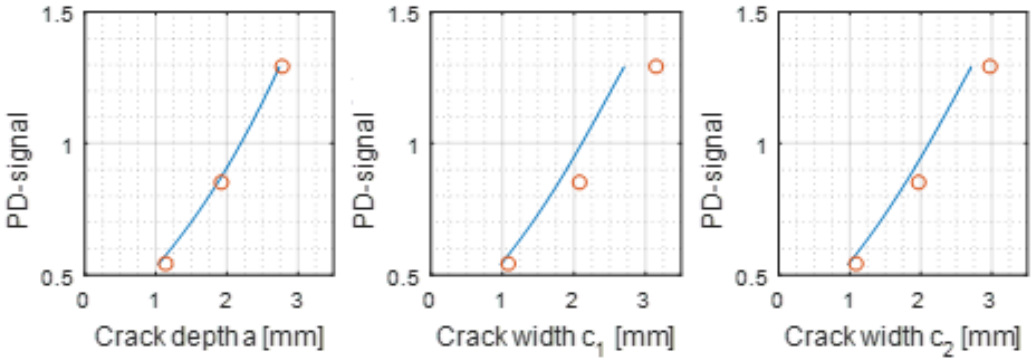

Figure 4.4. Non-adjusted calibration curve (blue curve) and measured crack size values (red circles) compared for all three crack lengths of the Ti 6-4 AM test sample.

4.1.4 Motivation of curve adjustment

The PD-signals fluctuate, which leads to small variations between consecutive cycles. This decreases the accuracy of the recorded PD-signals. In addition, the heat-tinting also has an impact on the registered PD-signals due to the added oxide layer that clogs the crack, affects the closure, and thereby changes the magnitude of the PD-signal when the test is resumed. A so called buzzing procedure is performed to shake off the oxide layer from the clogged crack. However, this disturbs the continuity of the test. Also, when attaching the wires to measure the PD-signals over the crack, the distance between the wires should be kept according to protocol since it has a direct impact on the resistance, and thus the registered PD-signals. Other possible sources of uncertainties and errors for crack growth testing of a typical superalloy at room temperature can be seen in Table 4.7 below. This table is formulated by Georgsson (2000). Type A errors are uncertainties that can be evaluated (and thereby mitigated) by statistical means while type B must be evaluated by other means. 1 indicates a major contribution, 2 a minor contribution and 0 no contribution to the respective parameters.

Table 4.7. Typical sources of uncertainty and their likely contribution to uncertainties on evaluated fatigue crack growth, according to Georgsson (2000).

Source of uncertainty	Type[1]	a	ΔK	da/dN
1. Test piece				
Dimension of the specimen	A or B	0	2	0
Distance between the measuring wires	A	1	2	0
Distance between the reference wires	A	2	2	0
2. Test system				
Alignment	B	2	1	0
Uncertainty in force measurement	B	0	1	0
Drift in force measuring system	B	0	2	0
Variation of the PD-signal due to noise, amplification, PD-source etc.	A	2	1	1
3. Environment				
Laboratory ambient temperature and humidity	B	2	2	0
4. Test Procedure				
Measuring the calibration specimen's crack length	A or B	2	2	0
Calibration curve	A	1	1	0
Repeatability of measurement	A	1	1	0

The crack size can be hard to determine using optical microscopy. The heat-tinted area often has blurry boundaries which make the front of the crack size difficult to define. This is less of an issue for forged specimens that have a smaller grain size compared to cast specimens whereby the heat-tinted areas are easier to define. As all measurements of heat-tinted areas are done manually, the perceived edge of the crack is also measured to different lengths by different individuals, see Table 4.8. Further, the microscope used to measure the crack sizes has a certain accuracy that may vary between microscopes.

Table 4.8. Post-test measurements of the AM-specimen by three different individuals.

	a_n	b_n	c_{1f}	c_{2f}	a_f
Individual A	0.524	1.169	3.134	2.960	2.749
Individual B	0.520	1.174	3.151	2.952	2.763
Individual C	-	-	3.143	2.970	2.766

An additional source of uncertainty could be that different crack propagation test conditions contribute to different amount of strain at the crack tip. In the case of a test where the *R*-value, temperature and load are such that the strain at the crack tips is relatively large when the crack is fully opened, the PD-signal could get magnified causing an overestimation of the crack size. This has not been confirmed experimentally, but could if present have an impact on the translation between the PD-signal and the crack size for some conditions.

Errors may also depend on the material itself, and the variations which exist between specimens. Some material imperfections are to be expected along with small geometrical deviations and irregularities which may cause difference in fatigue endurance, according to Andersson (1991). One example is the material texture of the specimen, which is not exactly the same between different specimens and slightly affects how the crack grows.

The implifications presented in this section are some of the reasons why an absolute calibration curve can not be used and has to be adjusted according to the procedure of CCA.

4.2 Investigation of errors related to different test suppliers

In this part, the effect of shifting PD-signals supplied by Lab A and Lab B to match the interval of the calibration curve is evaluated. First the magnitude of error of Kb-specimens tested locally is investigated, to get an understanding of the margins of errors related to the determination of a_s and a_f. These magnitudes of error will then be compared to the method when the PD-signals from Lab A and Lab B are adjusted to a_s and a_f before the CCA method is used. This procedure will give an exact match to a_s, as explained in section 3.3. Therefore only adjustments to match the supplied PD-signals to the measured a_f are evaluated.

4.2.1 Errors related to GKN tested specimens

The reason why the calibration curve cannot be used without adjustment is realized by studying Figure 4.5. The spread in the two clusters of data, illustrated by the black rings and the blue stars at a_s and a_f, respectively, shows that an absolute calibration curve without adjustment fails to predict the actual crack sizes for most specimens.

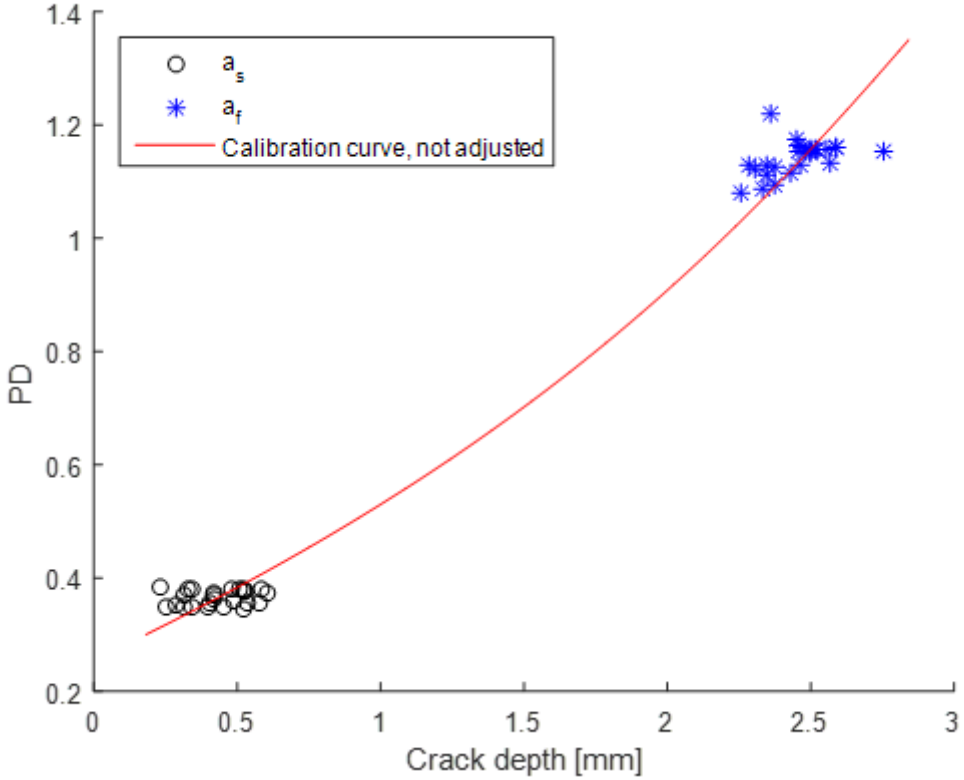

Figure 4.5. Measured PD-values corresponding to a_s and a_f for 25 Kb-specimens plotted against the unadjusted calibration curve for forged Ti 6-4.

The distribution of errors, or difference between values predicted by the unadjusted calibration curve and measured values for 25 Kb-specimens, can be seen in Figure 4.6. The average and extreme errors are show in Table 4.9 below.

Table 4.9. Average and extreme errors related to a_s and a_f of 25 Kb-specimens.

	Average error [mm]	Extreme error [mm]
a_s	0.0019	0.2705
a_f	0.0177	-0.2602

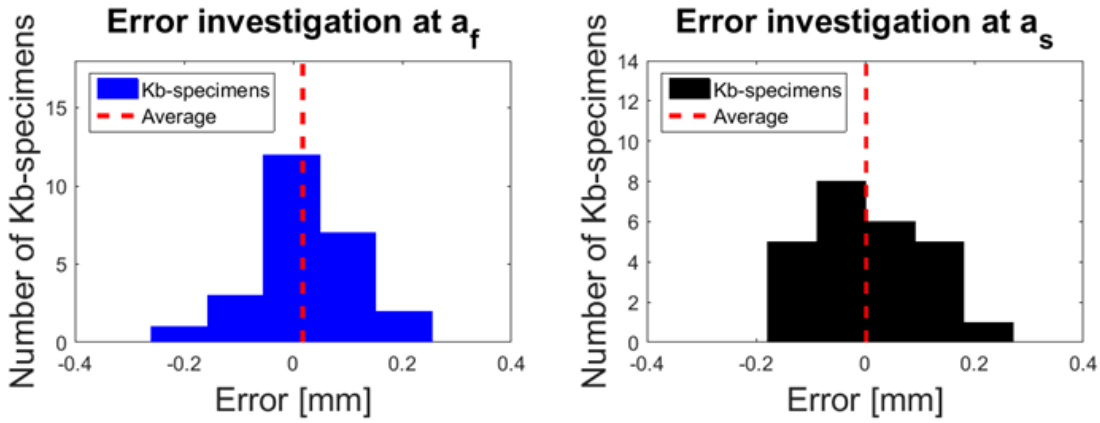

Figure 4.6. Errors of 25 Kb-specimens related to a_f and a_s.

4.2.2 Errors related to external specimens

By shifting the PD-signals supplied by Lab A and Lab B by a constant PD magnitude, the PD range can be made to match the valid range of the calibration curve, as shown in step 2 in Figure 3.5. It can be seen that the curve ends at a different crack depth than a_f. This is adjusted by using the CCA. Ten Kb-specimens from Lab A and nine Kb-specimens from Lab B were used to investigate the difference between measured and predicted crack depths after the data shift (that is, before CCA). The error was quantified as the difference between the measured and predicted values, after the shift of the PD-signals.

The error distribution of the investigated Kb-specimens can be seen in Figure 4.7. The errors that CCA has to correct are found to be larger for Lab A than for Lab B. Table 4.10 presents average and maximum errors for data from both laboratories. Both errors are higher than errors from GKN testing. Note also the systematic skewing towards positive errors.

Table 4.10. Average and max errors between shifted calibration curve and measured values of Kb-specimens supplied by Lab A and Lab B.

Supplier	Average error [mm]	Max error [mm]
Lab A	0.7000	1.1842
Lab B	0.4341	0.6824

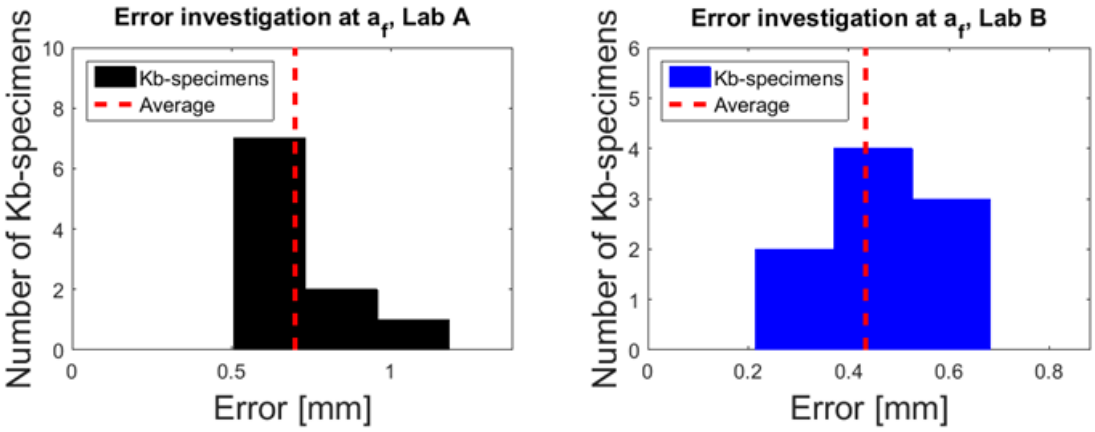

Figure 4.7. Error distribution of Kb-specimens supplied by Lab A and Lab B.

4.3 $CCA_{Lab\ A}$

The fact that Lab A performs several heat-tints during crack propagation tests to enable measurements (both in the a and c directions) was used to investigate how accurate the crack size could be predicted by the procedure of shifting PD-signals, to match the interval of the calibration curve based on GKN data, and then using CCA to adjust the curve to match a_f.

The data from nine Kb-specimens supplied by Lab A were used to create a new calibration curve. This way, the procedure of shifting the PD-signals to match the calibration curve of GKN, CCA_{GKN}, would not be necessary. The correlation between

PD-signals and crack size would instead be based on the PD-range according to Lab A. It was assumed that these specimens had similar notch sizes and that the measuring wires were correctly instrumented on the specimens.

These nine Kb-specimens contained a total of 56 PD-signals related to measured crack sizes. All Kb-specimens except Kb30 (marked with circles), which was deviating significantly in crack growth, were used to create the calibration curve, see Figure 4.8. This calibration curve is also based on a third degree polynomial function, where the data has been fitted in a least-square sense using MATLAB. With Kb30 excluded, there were 51 PD-signals and corresponding crack lengths, compared to the 20 used to create the calibration curve of GKN. The larger population of Kb-specimens implies that the crack growth should be better captured by the calibration curve designed for Lab A than for the one designed for GKN.

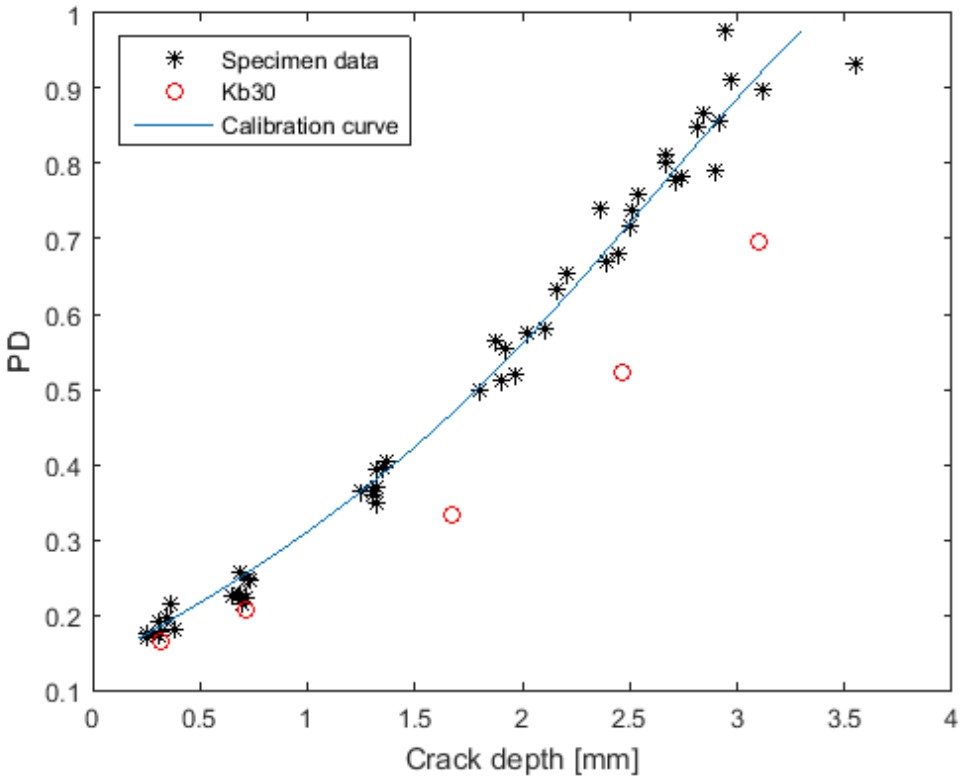

Figure 4.8. Calibration curve for Lab A.

4.3.1 Comparison between the different methods

All three methods of evaluating crack depth as a function of PD-signals for samples from Lab A; shifted and adjusted, linear and $CCA_{Lab\ A}$, are compared in Appendix V. All curves are connected to measured a_s and a_f magnitudes. There is thus no error between predicted and measured crack depth for a_s and a_f. These are therefore excluded from the error investigation. In Appendix V, the second point in the PD versus crack depth figure corresponds to point 1 in the bar diagram found in the appendix, the third corresponds to point 2 and so on.

All nine Kb-specimens were evaluated. The shifted and adjusted method proved to better predict the crack size for 36 out of a total of 38 measurements, i.e. in almost 95% of the cases, when compared with the linear method. This implies that the method of shifting the PD-signals, as supplied by Lab A, to match the interval of the calibration curve designed for GKN and then adjusting the curve to match the measured a_f is more accurate, compared to assuming a linear relation between PD-signals and crack size.

The results from the comparison of $CCA_{Lab\ A}$ and the shifted and adjusted (and also the linear) method should be interpreted with caution: since the calibration curve is created with data from eight out of nine Kb-specimens that are being evaluated, the only unbiased Kb-specimen is Kb30. For this specimen $CCA_{Lab\ A}$ proved to be the method that predicted the crack size best, followed by the shifted and adjusted method, and the linear method being the least accurate. Note however that Kb30 had a significantly deviating crack growth trend. Still, the investigation together with results of the cases for which CCA_{GKN} has been evaluated, indicates that the method of using an adjustable calibration curve gives more accurate predictions.

4.4 Crack size versus number of cycles

Using CCA to interpret crack size as a function of PD-signals gives a more conservative prediction as concluded earlier in the report. This means that the number of cycles required to reach a certain predicted crack depth or width occurs earlier than for the linear method, as seen in Figure 4.9. Considering the fact that the CCA method has been proven to be more accurate, compared with the linear method, an implementation of the CCA method would improve the safety margins.

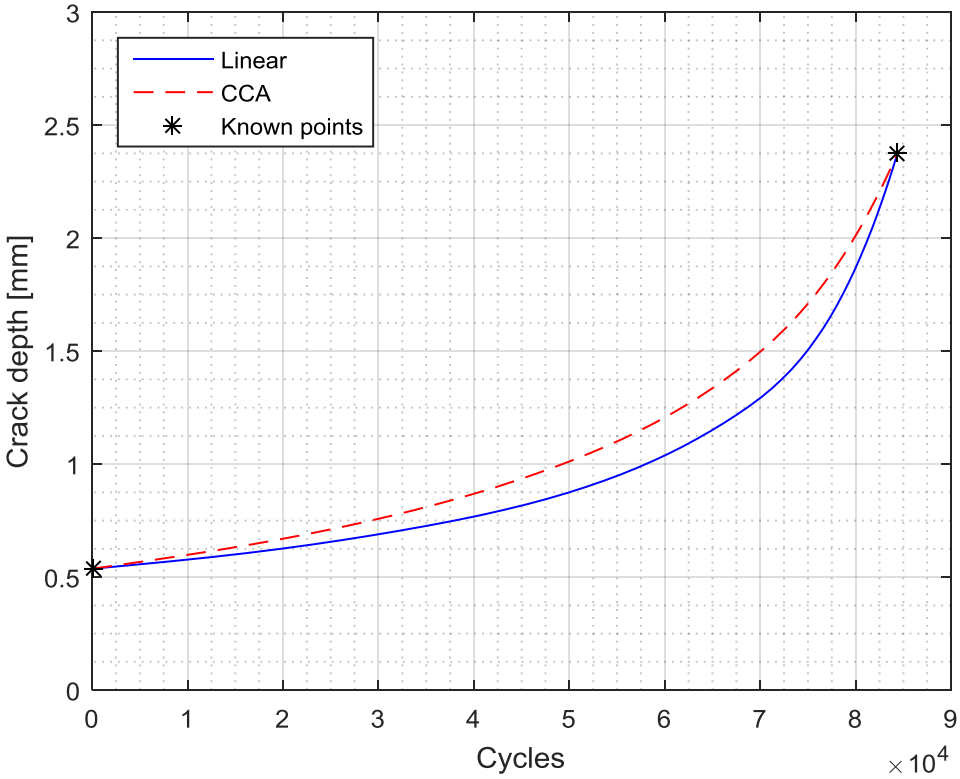

Figure 4.9. Crack depth versus number of cycles for linear method and CCA method, Ti 6-4 specimen.

4.5 Crack growth per cycle and stress intensity factor

Comparing the CCA method with the linear method the derived Paris curve in the $\mathrm{d}a/\mathrm{d}N$ versus ΔK plot (as in Figure 4.10) will have a less steep slope, corresponding to a lower m-magnitude in equation (2.8), when using CCA. This means that the crack growth rate for smaller ΔK values is predicted to be higher up to an intersection point, after which the crack growth rate will be lower compared to the linear method, see Figure 4.10 below for clarification.

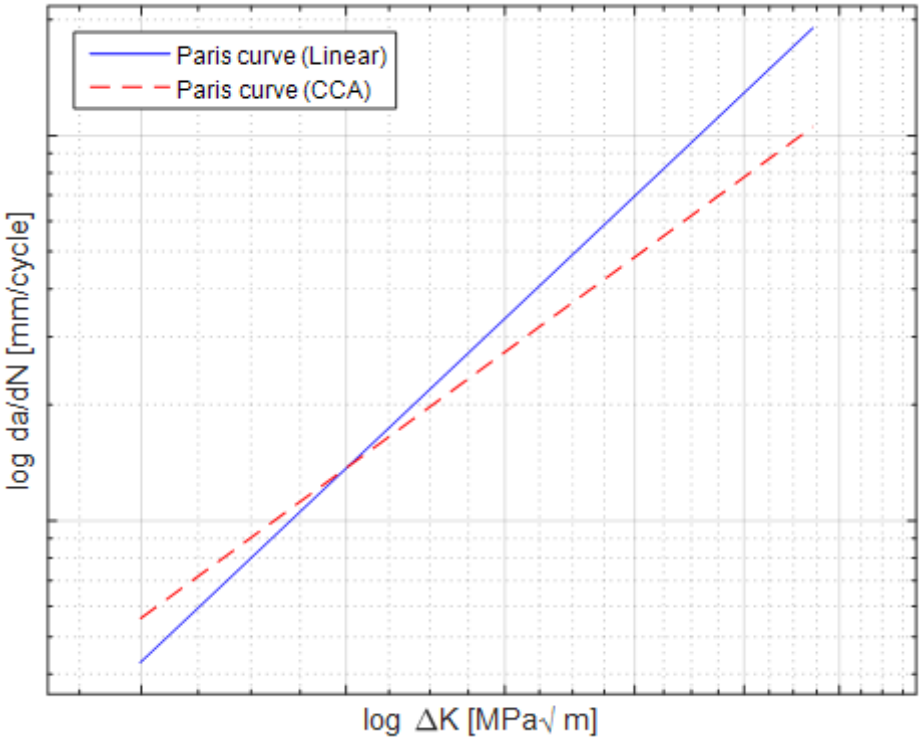

Figure 4.10. Estimated crack growth per cycle versus stress intensity ranges for the linear and the CCA methods.

4.5.1 Impact due to filtering

As seen in Figure 4.11, data can be more evenly spread over the stress intensity range by distributing the data points logarithmically. This can be done using SLM (described in section 3.4). In this manner, the number of evaluation points is easier to control and the specimens receive a more equal contribution to the calibration of the Paris curve, as every specimen receives the same weight. Further outliers are removed as the generation of data is based on a mathematical function describing the behavior of the crack growth.

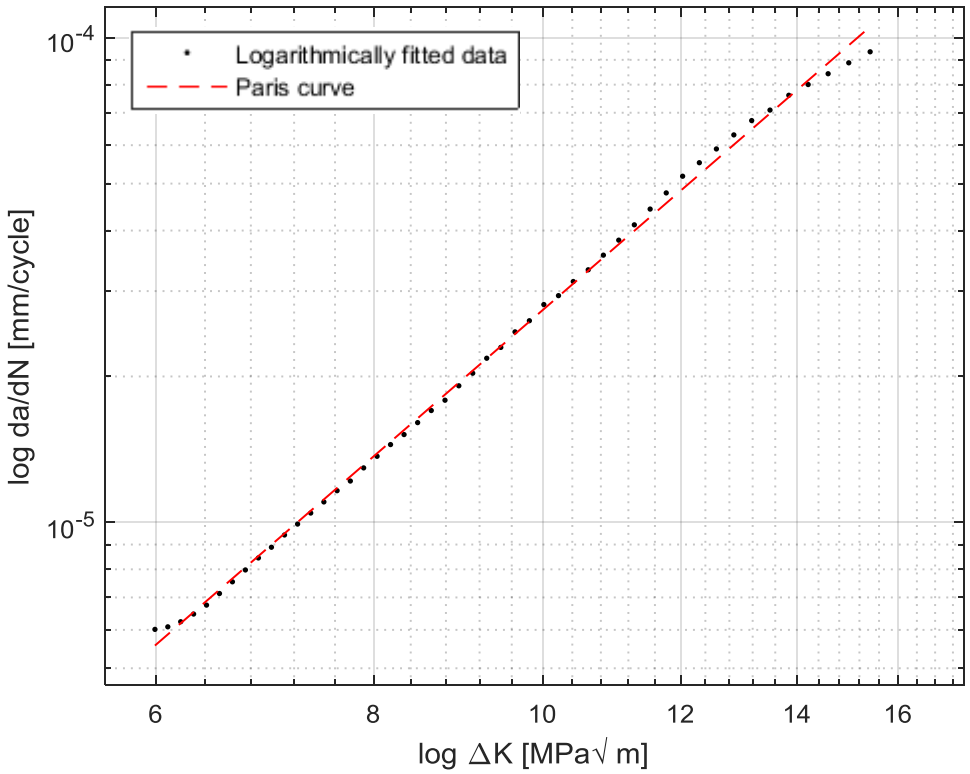

Figure 4.11. Resulting crack growth versus stress intensity range using SLM and adopting a logarithmical distribution.

There are some issues with this method: It depends on having a large enough amount of data points to find values with a good distribution. Further, the data points are less related to the original test data, due to the fact that a mathematical model is created using SLM and the logarithmic distribution. There may thus be a risk that the resulting data becomes too different from the original test data and provides invalid results. This may especially be a problem for smaller data sets with far fewer original data points compared with the resulting data points, after the transformation to a logarithmical distribution.

By using SLM, the data is (as mentioned) effectively filtered and outliers are removed, eliminating the need to manually adjust the data. However, the method sometimes provides values which give a deviating shape of the $\mathrm{d}a/\mathrm{d}N$ versus ΔK data, see Figure 4.12. The deviating behavior is affected by number of knots (or "breaks") where one part of the spline transitions into another. The number of knots may be adjusted for a better fit which may avoid these deviations. It may also depend on the type of polynomial which is modeled, in this case hermite.

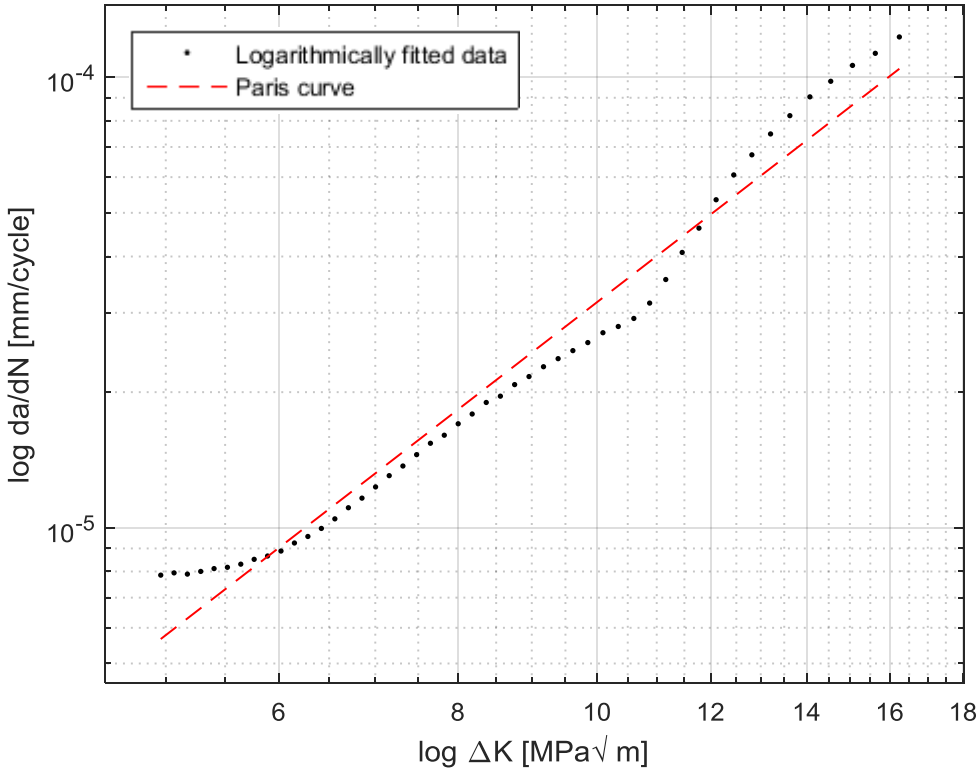

Figure 4.12. Crack growth versus stress intensity range with erratic (curvy) behavior.

4.6 Predictions using NASGRO and evaluation of A/P data

The two sets of data compared in the A/P plot in Figure 4.13 were both created using the same unadjusted GKN data. One set was created using the linear method while the other using the CCA method, each containing a total of 25 specimens (N).

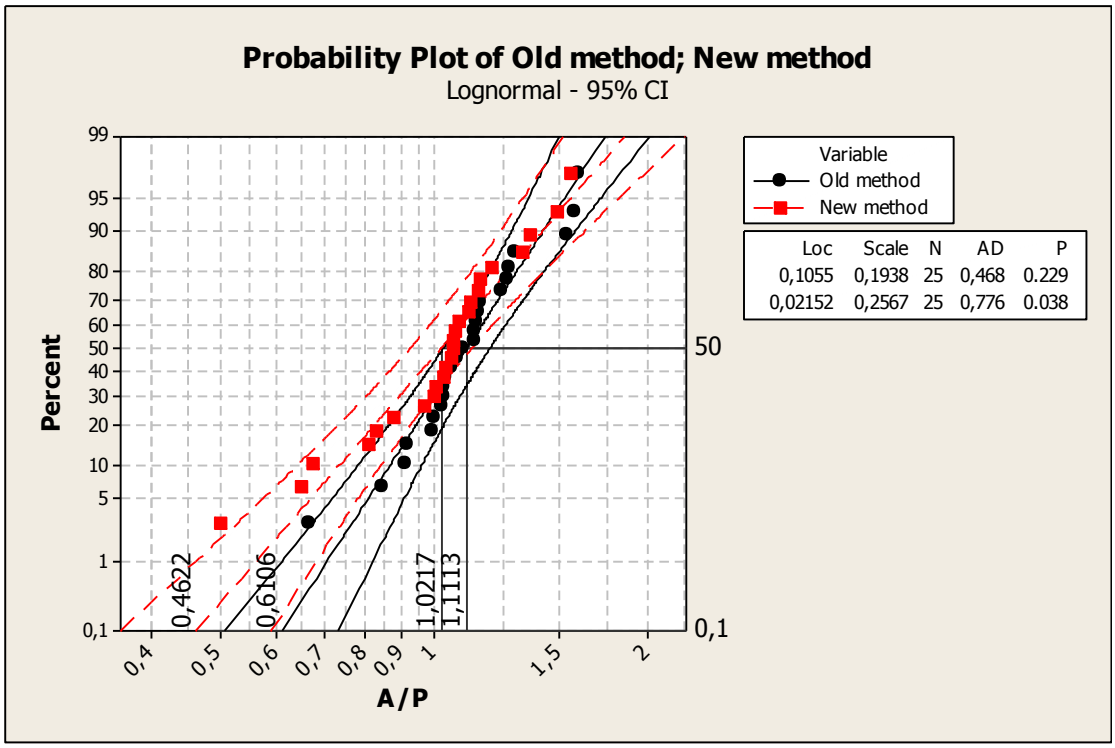

Figure 4.13. A/P plots of results from linear method, called "Old method", and CCA, called "New method".

The new method resulted in a higher scatter factor, indicating a poorer accuracy of the method but still within acceptable limits. A scatter factor between 2 and 3 is common, but a lower value is better. The scatter factors were calculated according to equation (3.11) and are presented below. The poorer accuracy is also supported by the lower value of the p-statistic (P) and the larger value of the Anderson-Darling statistic (AD). However, the shift (Loc) of the data for the new method is lower compared with the old method, which is desirable as it indicates a higher accuracy at 50% probability. The spread (Scale) of the data was higher for the new method. This can clearly be seen in Figure 4.13.

$$SF_{\text{Old}} = \frac{1.1113}{0.6106} = 1.82$$

$$SF_{\text{New}} = \frac{1.0217}{0.4622} = 2.21$$

These results show that the new method does not provide a smaller SF, but due to the small number of specimens (significantly smaller than usually studied) an increase in SF for the alternative method is not completely established. In order to achieve more reliable and statistically significant results, a sample of 12 specimens per temperature would be needed. In this case it would result in 48 specimens as four temperatures are considered. While it is unlikely that this would greatly change the SF-values, the result would be more reliable and provide a better verification of the analysis.

The cause of the higher SF may be in part due to the fact that the data is not adjusted, which means that some deviating data may be included and not removed. Another

possible reason relates to uncertainties with NASGRO predictions. As seen in Figure 4.13 above where some points are far from 1, the prediction made by NASGRO is sometimes far from the actual fatigue life. The software makes some simplifications. As an example the crack width is taken as an average between the two directions c_1 and c_2, which presumes the crack growth to be symmetrical, this assumption is often not the case. Also, the software models the ratio between crack depth and crack width to go approximately from 1 to 0.6. This is often not the actual ratio in reality. The true case of the differences may be in NASGRO itself and it may also be in the specimen testing, with all the uncertainties it brings.

It has been shown that CCA makes a more accurate prediction for the crack depth and width and should therefore give a better A/P plot if the lifespan of the specimens would be set to a lower value. However, since there were no measured value between a_s and a_f in the evaluated data, it was not possible to evaluate if this affected the results.

5 Conclusions

A new method based on an adjustable calibration curve, CCA, has been proven to be more accurate than the currently used linear method. In some of the evaluated cases it has overestimated the crack size, making it too conservative (i.e. increasing the safety margins). The linear method on the other hand almost always underestimates the crack size, which can lead to lower safety margins. Based on the analysis performed, CCA also seems to be not significantly affected of whether the material is Ti 6-4 or IN718. This means that it is (at least within reasonable limits) not restricted to a single type of material, which increases its flexibility. It is however less robust than the current linear model in the sense that it is limited to a certain range of PD-signal magnitudes. In contrast the linear method is able to handle any PD-signals, without the risk of major errors.

The method of shifting and adjusting PD-signals obtained from Lab A and Lab B to match the PD-interval of a calibration curve obtained from GKN data has also been proven to be more accurate than the linear method. Of the evaluated Kb-specimens with several measured crack sizes for each specimen supplied by Lab A, the shifted and adjusted method proved to be more accurate in almost 95% of the cases, see Appendix V for details. The same evaluation was not performed for Lab B, but based on the outcome from the evaluation of the Lab A specimens and the fact that the same procedure is being used to handle Lab B data, the assumption was that that the crack size would be predicted more accurately also for these specimens. This means that even though the accuracy of predicting crack size is not as great as for specimens tested at GKN, the data supplied from Lab A and Lab B can be used and interpreted better than with the current linear method.

A calibration curve based on Lab A data has been developed. It has the advantage of being adjusted to the measured crack sizes from Lab A. This means that no shifting is needed to adapt the magnitude of the PD-signals from Lab A as is the case when a calibration curve based on GKN data is used. The evaluation of the accuracy of $\mathrm{CCA}_{\mathrm{Lab\,A}}$ in Appendix V should be interpreted with caution, since the calibration curve is derived from the same specimens as those being evaluated. The only unbiased specimen is Kb30, for which $\mathrm{CCA}_{\mathrm{Lab\,A}}$ predicted the crack sizes most accurately of the three different methods. This indicates that it probably is the best method. However the Kb30 specimen showed an uncharacteristic crack growth pattern. Thus, more Kb-specimens need to be evaluated to draw definitive conclusions. One advantage with using $\mathrm{CCA}_{\mathrm{Lab\,A}}$ is that time can be saved in evaluating Kb-specimens. The many heat-tints during the crack propagation tests, which Lab A performs to ensure that the crack is growing as predicted by the analytical solution according to Roe-Coffin, could be avoided. Instead only two heat-tints would be needed to measure a_{s} and a_{f}, which are used to adjust the calibration curve. This way the efficiency of the crack propagation tests could be improved, saving time and resources.

The weighting of the data points before fitting them to the log-log curve where Paris law is valid has not been completely evaluated. Further investigations are needed. Shape Language Modeling, SLM, has the potential to be of good use in eliminating the need for manual adjustment of data, i.e. remove so-called outliers, as well as

filtering data. However, it has some flaws and introduces some risks. In its current form it is not deemed superior to the presently used method of filtering. However, using SLM opens up the possibility to more evenly distributed data points to establish the Paris curve while also achieving a proper weighting of all specimen data sets.

When analyzing the A/P plot and scatter factor, the linear method gives a better result. However, due to the small data set it cannot be established with certainty that the result is statistically significant. A more extensive analysis is needed with adjusted data as well as an increased amount of specimens. In addition to this the current NASGRO implementation, which is used to obtain the predicted fatigue life, should be evaluated and an analysis of influencing uncertainties carried out.

5.1 Future work

There are several areas in which the future work can be focused. The CCA method itself can be improved by increasing the population of Kb-specimens that are used to create the calibration curve. This way the crack growth behavior could be better captured. This includes a better evaluation of scatter in crack growth characteristics that can be contrasted to predict crack growth lives. Furthermore the crack growth can probably be described by another mathematical function that predicts the crack size better than a third degree polynomial equation.

The adjustments and procedures done manually to handle data could be improved. The procedure of handling raw test data from the test machines to create the crack size versus number of cycles and $\mathrm{d}a/\mathrm{d}N$ versus ΔK plots is rather complicated. This procedure could be automated, which would increase the efficiency of the procedure and reduce the risk of handling errors.

A calibration curve for Lab B could be created just as the ones created for GKN and Lab A. By heat-tinting each specimen four times and registering the PD-signals at which the heat-tints are performed, the PD-signals could be coupled to the corresponding crack sizes when evaluated post-testing. A calibration curve created in this manner for Lab B would eliminate the need for shifting data. Further, the accuracy would likely be improved.

By using the CCA method to evaluate forged IN718 specimens to the same extent as the forged Ti 6-4 specimens, the robustness of the method can be further examined. As the CCA method was able to predict the crack size of the calibration specimens made of forged IN718 more accurately than the linear method, it could most likely be shown that it is robust enough to be used for a complete evaluation of this material as well. Furthermore, cast materials could be examined which have a microstructure that differs from forged specimens. This would indicate e.g. if the grain size of the Kb-specimens have an impact on the ability of the derived CCA to predict crack size.

The A/P evaluation could be significantly improved by expanding the sample size. By having at least 12 specimens per temperature the results will become statistically significant. In the case of the studied forged Ti 6-4 specimens it would mean adding specimen data from Lab B and Lab A. For Lab B it would require an extra adjustment in order to shift the PD-signals to a range that the CCA method is able to handle. For

Lab A, the separate calibration curve designed specifically for Lab A data could be used. Apart from adding more specimens, the data will also need to be filtered, where deviating $\mathrm{d}a/\mathrm{d}N$ versus ΔK data points are removed. Adjusted data, where outliers and deviating data points are manually removed, will change the results. It is unclear how significant such a change may be, and due to the unexpected result – where the CCA based data did not provide a better SF – it is relevant to examine and verify the evaluation. Finally, the filtering procedures using SLM need to be revised and improved.

6 References

Adams, R., Essex, C. (2010): *Calculus: a complete course*. Pearson Canada Inc., Toronto Canada, 973 pp.

Andersson, H. (1991): *Kompendium i Utmattning*. Chalmers Tekniska Högskola, Göteborg, Sweden, 213 pp

Andrew, M. (2016): *Brittle Fracture*. Retrieved from: http://www.doitpoms.ac.uk/tlplib/brittle_fracture/printall.php (2016-05-14)

ASTM International (2004): *Annual Book of ASTM Standards 2004, Section 3: Metals Test Methods and Analytical Procedures*, Volume 03.01: Metals-Mechanical Testing; Elevated and Low-Temperature Tests; Metallography. ASTM International, West Conshohocken, Pennsylvania, United States, 682 pp.

ASTM (2015) E647-15, *Standard Test Method for Measurement of Fatigue Crack Growth Rates*, ASTM International, West Conshohocken, PA, 2015.

D'Errico, J (2009, June 15): *SLM – Shape Language Modeling.* Retrieved at: http://www.mathworks.com/matlabcentral/fileexchange/24443-slm-shape-language-modeling (2016-02-15)

Dowling, N. (2013): *Mechanical Behavior of Materials*. Pearson Education Limited, Essex, England, 954 pp.

Gandossi, L., Summers, S. A., Taylor, N. G., Hurst, R. C., Hulm, B. J., Parker, J. D. (2001): *The potential drop method for monitoring crack growth in real components subjected to combined fatigue and creep conditions: application of FE techniques for deriving calibration curves*, International Journal of Pressure Vessels and Piping 78 (2001) 881—891.

Georgsson, P. (2000): *The Determination of Uncertainties in Fatigue Crack Growth Measurement*. Standards Measurement & Testing Project No. SMT4-CT97-2165, Volvo Aero Corporation, Trollhättan, Sweden, 23 pp.

Kleinbaum, D. G., Kupper, L. L., Muller, K. E., Nizam, A. (1998): *Applied Regression Analysis and Other Multivariable Methods*. Duxbury Press, California, United States, 798 pp.

Jensen, A (1999): *Elektrisk FE-analys av sprickpropageringsmätning med Potential Drop metoden?* Document 1999VAC004826, Volvo Aero Corporation, Trollhättan, Sweden, 25 pp.

MathWorks (2016): *Polynomial curve fitting – MATLAB polyfit*. Retrieved from: http://se.mathworks.com/help/matlab/ref/polyfit.html (2016-03-10).

Minitab (2016a): *The Anderson-Darling statistic.* Retrieved from: http://support.minitab.com/en-us/minitab/17/topic-library/basic-statistics-and-graphs/introductory-concepts/data-concepts/anderson-darling/ (2016-04-11)

Minitab (2016b): *What is a p-value?*. Retrieved from: http://support.minitab.com/en-us/minitab/17/topic-library/basic-statistics-and-graphs/introductory-concepts/p-value-and-significance-level/what-is-pvalue/ (2016-04-13)

Newman, J. C., Raju, I. S. (1981): *NASA Technical Memorandum 83200, Stress-intensity factor equations for cracks in three-dimensional finite bodies*. NASA, Hampton, Virginia, USA, 49 pp.

SME (2016): *Electrical Discharge Machining.* Retrieved from: http://www.sme.org/ProductDetail.aspx?id=80246 (2016-05-17)

Southwest Research Institute (2016): *NASGRO® Crack Growth Equation.* Retrieved from: http://www.swri.org/4org/d18/mateng/matint/nasgro/Overview/Equation.htm (2016-05-14)

Tarnowski, K., Davies, C. M., Nikbin, K. M., Dean, D. (2014): *The influence of strain on crack length measurements using the potential drop technique*, 2 pp. Retrieved from: http://www.icem16.org/resumes/r_F59ZVPS3.pdf (2016-03-10)

VanStone, R. H., Richardson, T. L. (1985): Potential-Drop Monitoring of Cracks in Surface-Flawed Specimens, *Automated Test Methods for Fracture and Fatigue Crack Growth, ASTM STP 877*, W. H. Cullen, R. W. Landgraf, L. R. Kaisand and J. H. Underwood, Eds., American Society for Testing and Materials, Philadelphia, United States 1985, 166 pp.

Weisberg, S. (2013): *Applied Linear Regression*. Wiley & Sons, Inc. Hoboken, United States, 370 pp.

Appendix I – Roe-Coffin solution

This appendix describes the Roe-Coffin potential solution for a semi-elliptical flaw having the geometry shown in Figure 2.2 and Figure 2.4. This solution can be used to determine the crack geometries from a normalized potential. The potential (V) is calculated as

$$V = V_0 L_\mathrm{p} \frac{\left[\frac{\sqrt{1-k^2\sin^2\theta}}{\tan\theta}\right] + E(k,\theta) - Q}{E\left(k,\frac{\pi}{2}\right) - Q}$$

where

$V_0 = \text{remote potential}$

$E(\delta_1, \delta_2) = \int_0^{\delta_2} (1 - \delta_1^2 \sin^2\phi)^{1/2} \mathrm{d}\phi,$

$\theta = \tan^{-1}\left(\sqrt{a}\right)$
$\theta_0 = \tan^{-1}(b/\beta)\,, \text{and}$

$Q = E(k, \theta_0) + \frac{b\beta^2}{ac\gamma}$

There are two solutions for α, β, γ, and k depending on whether the crack aspect ratio is greater or less than unity. Within those two solutions and the value of α varies depending on the relative difference between crack dimensions and probe spacing. The parameter z is the dimension by which the probe spacing is off the centreline of EDM defect.

For $c \geq a \geq b$

$$\beta^2 = a^2 - b^2$$
$$\gamma^2 = c^2 - b^2$$
$$k^2 = 1 - \beta^2/\gamma^2$$

If $L_\mathrm{p}^2 + z^2 \geq \gamma^2$

$$\alpha = \frac{1}{2}\left[\frac{L_\mathrm{p}^2 + z^2 - \gamma^2}{\beta^2} + \sqrt{\left(\frac{L_\mathrm{p}^2 + z^2 - \gamma^2}{\beta^2}\right) + \frac{4\gamma^2 L_\mathrm{p}^2}{\beta^4}}\right]$$

If $L_\mathrm{p}^2 + z^2 < \gamma^2$

$$\alpha = \frac{2\gamma^2 L_\mathrm{p}^2/\beta^4}{\frac{\gamma^2 - L_\mathrm{p}^2 - z^2}{\beta^2} + \sqrt{\left(\frac{\gamma^2 - L_\mathrm{p}^2 - z^2}{\beta^2}\right) + \frac{4\gamma^2 L_\mathrm{p}^2}{\beta^4}}}$$

For $a > c > b$

$$\beta^2 = c^2 - a^2$$
$$\gamma^2 = a^2 - b^2$$
$$k^2 = 1 - \beta^2/\gamma^2$$

If $L_\mathrm{p}^2 + z^2 \geq \beta^2$

$$\alpha = \frac{1}{2}\left[\frac{L_\mathrm{p}^2 + z^2}{\beta^2} - 1 + \sqrt{\left(\frac{L_\mathrm{p}^2 + z^2}{\beta^2} - 1\right)^2 + \frac{4L_\mathrm{p}^2}{\beta^2}}\right]$$

If $L_\mathrm{p}^2 + z^2 < \beta^2$

$$\alpha = \frac{2L_\mathrm{p}^2/\beta^2}{1 - \frac{L_\mathrm{p}^2 + z^2}{\beta^2} + \sqrt{\left(1 + \frac{L_\mathrm{p}^2 + z^2}{\beta^2}\right) + \frac{4L_\mathrm{p}^2}{\beta^2}}}$$

The only unmeasured parameter in this solution is V_0; however, the potentials are normalized by V/V_n so V_0 can be eliminated.

Close to the EDM notch, the influence of the height (b) of the EDM notch is considered. The algorithm used uses the total potential V as a function of the potential solution for a crack (V_ca), the potential of a notch (V_n) and the potential of a crack having the size of the notch (V_cn):

$$V = V_\mathrm{ca} + Q(V - V_\mathrm{cn})$$

For $a_\mathrm{n} > a > 2a_\mathrm{n}$

$$Q = \left(2 - \frac{a}{a_\mathrm{n}}\right)$$

For $a > 2a_\mathrm{n}$

$$Q = 0$$

The value of b used to calculate V_ca and V_cn is zero. The experimentally measured b is used to calculate V_n.

Appendix II – NASA TM-83200 for semi-elliptical surface cracks

For specimens subjected to a remote tensile loading, the stress intensity factors can be found as functions of crack depth, crack length, parametric angle and plate thickness. These empirical equations were close to finite-element results, generally within 5 percent. The only exception was where the crack front intersects a free surface, creating something similar to a boundary layer. The equations are still expected to give adequate estimations in this region, assuming that the cracks are semi-elliptical surface cracks (Newman, Raju 1981).

$$\Delta K = \Delta S F \sqrt{\pi \frac{a}{Q}} \tag{A.1}$$

$$K_{\mathrm{I}} = S \sqrt{\pi \frac{a}{Q}} F_{\mathrm{S}} \left(\frac{a}{c}, \frac{a}{t}, \frac{c}{b}, \phi \right) \tag{A.2}$$

for $0 \leq a/c \leq 2$, $c/b < 0.5$ and $0 \leq \phi \leq \pi$. Q is the shape factor for the elliptical crack, found in equation (A.4) and (A.7), and F_{S} is the boundary-correction factor for surface crack in a plate, given by equation (A.3) below, as a function of depth a and width c of the crack, thickness t and half-width b of the plate and the parametric angle ϕ of the crack ellipse.

$$F_{\mathrm{S}} = \left[M_1 + M_2 \left(\frac{a}{t} \right)^2 + M_3 \left(\frac{a}{t} \right)^4 \right] g f_{\phi} f_{\mathrm{W}} \tag{A.3}$$

Where M_{i} and g are curve fitting functions presented in equation (A.4), f_{w} is the finite-width correction factor , see equation (A.6), and f_{ϕ} is the angular function derived from embedded elliptical crack solution, see equation (A.5).

For $\frac{a}{c} \leq 1$:

$$\begin{aligned} M_1 &= 1.13 - 0.09 \left(\frac{a}{c} \right) \\ M_2 &= -0.54 + \frac{0.089}{0.2 + \left(\frac{a}{c} \right)} \\ M_3 &= 0.5 - \frac{1}{0.65 + \frac{a}{c}} + 14 \left(1 - \frac{a}{c} \right)^{24} \\ g &= 1 + \left[0.1 + 0.35 \left(\frac{a}{t} \right)^2 \right] (1 - \sin \phi)^2 \\ Q &= 1 + 1.464 \left(\frac{a}{c} \right)^{1.65} \end{aligned} \tag{A.4}$$

And

$$f_{\phi} = \left[\left(\frac{a}{c} \right)^2 \cos^2 \phi + \sin^2 \phi \right]^{\frac{1}{4}} \tag{A.5}$$

$$f_{\mathrm{W}} = \sec \left(\frac{\pi c}{2b} \sqrt{\frac{a}{t}} \right)^{\frac{1}{2}} \tag{A.6}$$

For $\frac{a}{c} \geq 1$:

$$M_1 = \sqrt{\frac{c}{a}}\left(1 + 0.04\frac{c}{a}\right)$$
$$M_2 = 0.2\left(\frac{c}{a}\right)^4$$
$$M_3 = -0.11\left(\frac{c}{a}\right)^4 \qquad \text{(A.7)}$$
$$g = 1 + \left[0.1 + 0.35\left(\frac{c}{a}\right)\left(\frac{a}{t}\right)^2\right](1 - \sin\phi)^2$$
$$Q = 1 + 1.464\left(\frac{c}{a}\right)^{1.65}$$

And

$$f_\phi = \left[\left(\frac{c}{a}\right)^2 \sin^2\phi + \cos^2\phi\right]^{\frac{1}{4}} \qquad \text{(A.8)}$$

And f_W as stated in equation (A.6).

Appendix III – Errors using CCA on calibration specimens

All values in the table below are given in mm. Point 2 indicate the second data point after the initial crack measurement and point 3 the data point before final crack measurement.

ERRORS		CCA method (Ti 6-4 curve)			GKN linear method		
		a	c1	c2	a	c1	c2
IN718							
IN-2	Point 2	*0.0595*	*0.0188*	*0.0240*	*0.2125*	*0.1490*	*0.1459*
	Point 3	*0.0091*	*-0.0290*	*0.0164*	*0.2210*	*0.1437*	*0.1794*
IN-3	Point 2	*0.0077*	*-0.0041*	*0.0014*	*0.0429*	*0.0263*	*0.0298*
	Point 3	-	-	-	-	-	-
IN-4	Point 2	*0.0033*	*0.0171*	*0.0055*	*0.1078*	*0.1077*	*0.0900*
	Point 3	*-0.0261*	*-0.0192*	*-0.0082*	*0.1024*	*0.0863*	*0.0913*
IN-5	Point 2	*0.0863*	*0.0426*	*0.0527*	*0.2691*	*0.1856*	*0.1888*
	Point 3	*0.0316*	*0.0319*	*0.0454*	*0.1419*	*0.1050*	*0.1177*
10	Point 2	*0.0556*	*-0.0414*	*-0.0611*	*0.2068*	*0.0878*	*0.0598*
	Point 3	*0.0228*	*-0.0790*	*-0.0794*	*0.2064*	*0.0651*	*0.0577*
	Max	0.0863	-0.0790	-0.0794	0.2691	0.1856	0.1888
	Mean	0.0278	-0.0069	-0.0004	0.1679	0.1063	0.1067
Ti 6-4							
Ti-5	Point 2	*-0.0148*	*-0.0093*	*-0.0088*	*0.1119*	*0.0969*	*0.0909*
	Point 3	*-0.0181*	*0.0193*	*-0.0056*	*0.1388*	*0.1349*	*0.1060*
Ti-10	Point 2	*-0.0492*	*-0.0358*	*-0.0300*	*0.1036*	*0.0839*	*0.0839*
	Point 3	*0.0009*	*0.0031*	*0.0021*	*0.044*	*0.0244*	*0.0249*
Ti-15	Point 2	*0.0258*	*0.0123*	*0.0216*	*0.1444*	*0.1186*	*0.1201*
	Point 3	*-0.0414*	*-0.0492*	*-0.0358*	*0.1230*	*0.0880*	*0.0930*
Ti-1	Point 2	*-0.0105*	*0.0344*	*0.0229*	*0.1976*	*0.2113*	*0.1884*
	Point 3	*-0.0075*	*-0.0028*	*-0.0136*	*0.1579*	*0.1297*	*0.1119*
Ti-20	Point 2	*-0.0234*	*-0.0663*	*-0.0497*	*0.1617*	*0.0772*	*0.0872*
	Point 3	*-0.0202*	*-0.0501*	*-0.0473*	*0.1522*	*0.0651*	*0.0664*
	Max	-0.0492	-0.0663	-0.0497	0.1976	0.2113	0.1884
	Mean	-0.0158	-0.0144	-0.0144	0.1335	0.1030	0.0973

ERRORS		CCA method (IN718 curve)			GKN linear method		
		a	c1	c2	a	c1	c2
IN718							
IN-2	Point 2	*0.0531*	*0.0432*	*0.0494*	*0.2125*	*0.1490*	*0.1459*
	Point 3	*0.0159*	*0.0245*	*0.0679*	*0.2210*	*0.1437*	*0.1794*
IN-3	Point 2	*0.0054*	*0.0005*	*0.0063*	*0.0429*	*0.0263*	*0.0298*
	Point 3	-	-	-	-	-	-
IN-4	Point 2	*-0.0045*	*0.0294*	*0.0193*	*0.1078*	*0.1077*	*0.09*
	Point 3	*-0.0236*	*0.0111*	*0.0213*	*0.1024*	*0.0863*	*0.0913*
IN-5	Point 2	*0.1043*	*0.1038*	*0.1096*	*0.2691*	*0.1856*	*0.1888*
	Point 3	*0.0691*	*0.1022*	*0.1075*	*0.1419*	*0.105*	*0.1177*
10	Point 2	*0.0483*	*-0.0185*	*-0.0370*	*0.2068*	*0.0878*	*0.0598*
	Point 3	*0.0399*	*-0.0187*	*-0.0232*	*0.2064*	*0.0651*	*0.0577*
	Max	0.1043	0.1038	0.1096	0.2691	0.1856	0.1888
	Mean	0.0412	0.0381	0.0431	0.1679	0.1063	0.1067
Ti 6-4							
Ti-5	Point 2	*-0.0167*	*0.0151*	*0.0157*	*0.1119*	*0.0969*	*0.0909*
	Point 3	*0.0117*	*0.0898*	*0.0582*	*0.1388*	*0.1349*	*0.106*
Ti-10	Point 2	*-0.0345*	*0.0150*	*0.0173*	*0.1036*	*0.0839*	*0.0839*
	Point 3	*0.0303*	*0.0489*	*0.0416*	*0.044*	*0.0244*	*0.0249*
Ti-15	Point 2	*0.0101*	*0.0178*	*0.0301*	*0.1444*	*0.1186*	*0.1201*
	Point 3	*-0.0427*	*-0.0159*	*-0.0028*	*0.123*	*0.088*	*0.093*
Ti-1	Point 2	*-0.0187*	*0.0682*	*0.0579*	*0.1976*	*0.2113*	*0.1884*
	Point 3	*0.0024*	*0.0446*	*0.0312*	*0.1579*	*0.1297*	*0.1119*
Ti-20	Point 2	*-0.0025*	*-0.0009*	*0.0108*	*0.1617*	*0.0772*	*0.0872*
	Point 3	*0.0367*	*0.0575*	*0.0480*	*0.1522*	*0.0651*	*0.0664*
	Max	-0.0427	0.0898	0.0582	0.1976	0.2113	0.1884
	Mean	-0.0061	0.0391	0.0333	0.1335	0.1030	0.0973

Appendix IV - Difference between measured and predicted crack sizes with respect to crack size

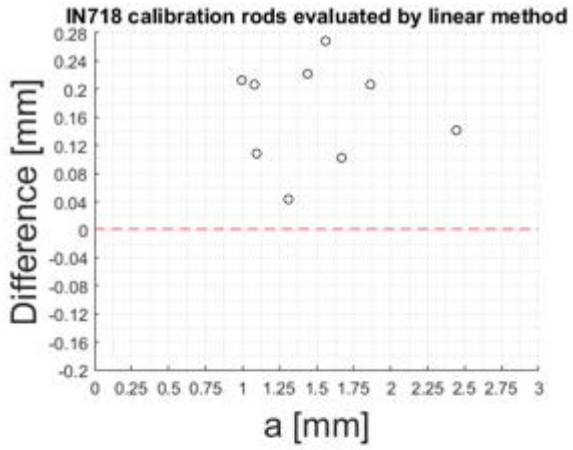

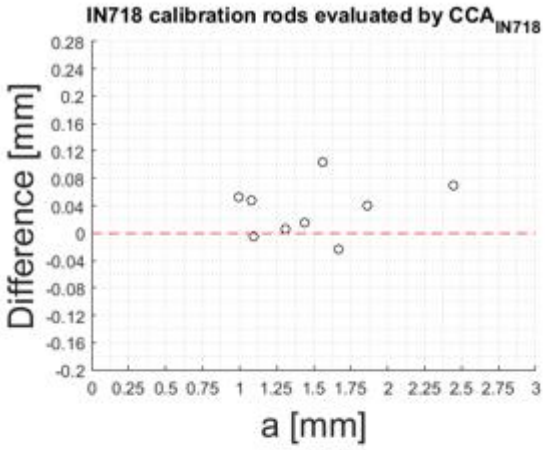

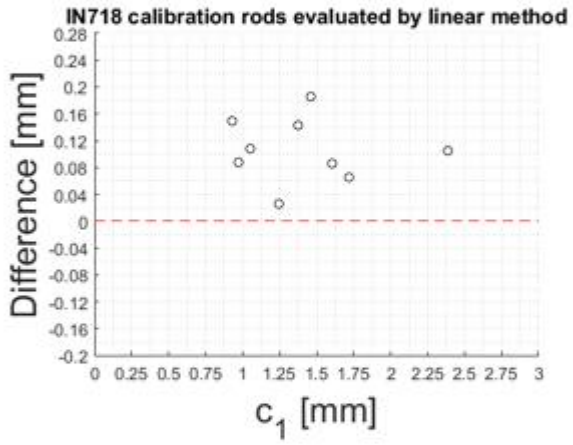

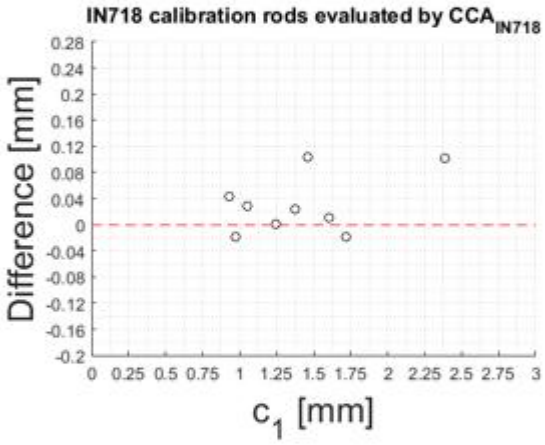

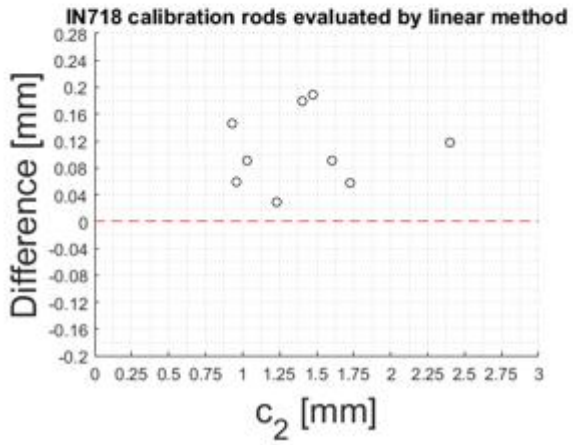

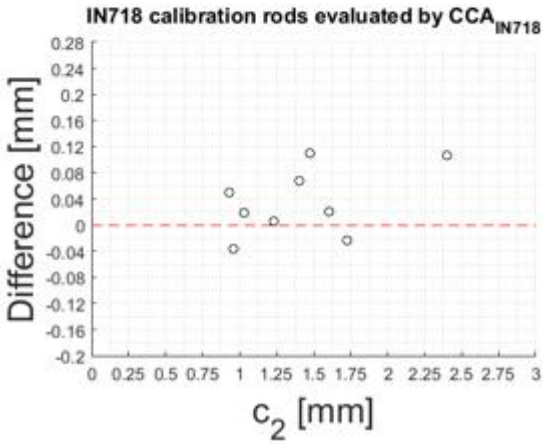

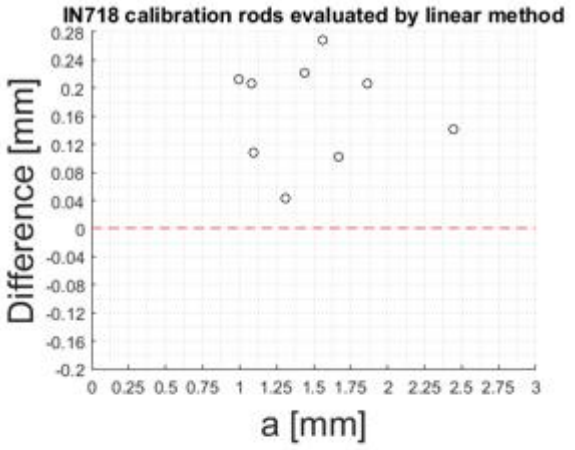
IN718 calibration rods evaluated by linear method
Difference [mm]
a [mm]

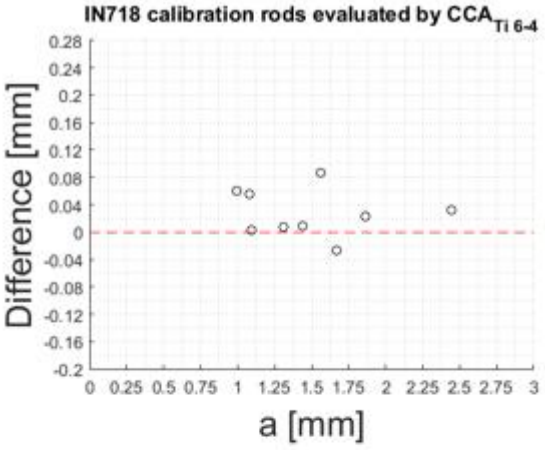
IN718 calibration rods evaluated by CCA Ti 6-4
Difference [mm]
a [mm]

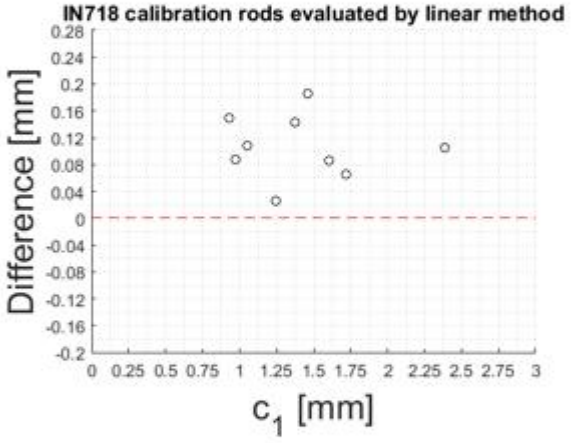
IN718 calibration rods evaluated by linear method
Difference [mm]
c1 [mm]

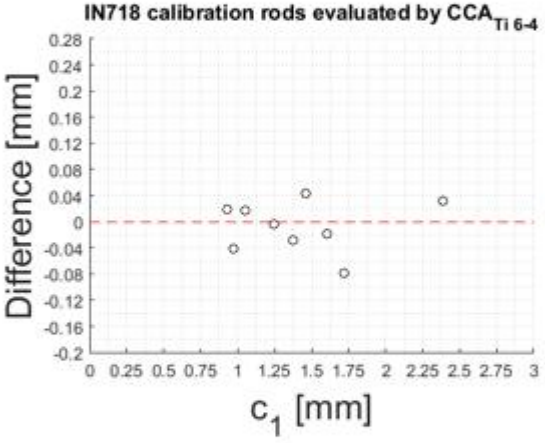
IN718 calibration rods evaluated by CCA Ti 6-4
Difference [mm]
c1 [mm]

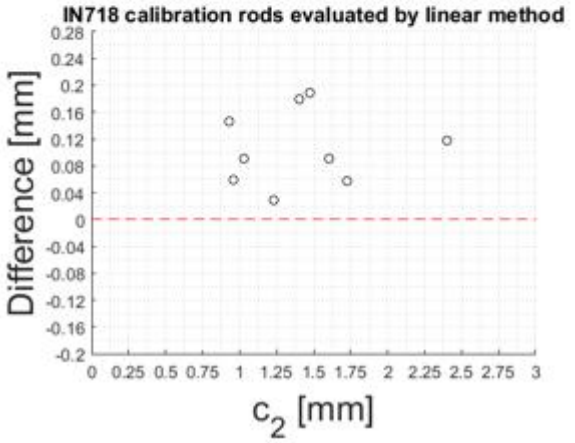
IN718 calibration rods evaluated by linear method
Difference [mm]
c2 [mm]

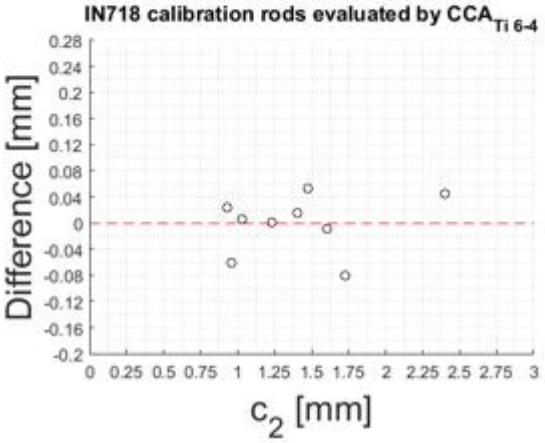
IN718 calibration rods evaluated by CCA Ti 6-4
Difference [mm]
c2 [mm]

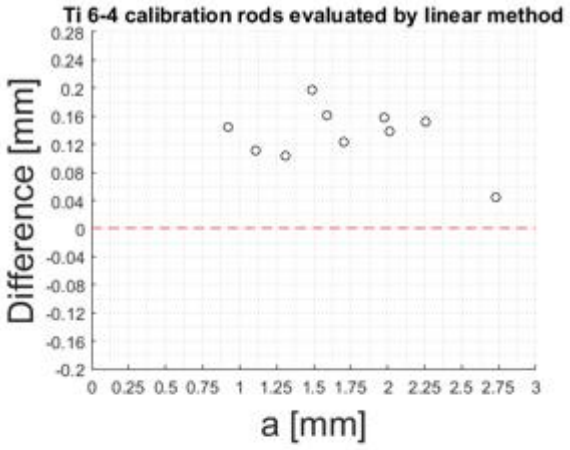
Ti 6-4 calibration rods evaluated by linear method
Difference [mm]
a [mm]

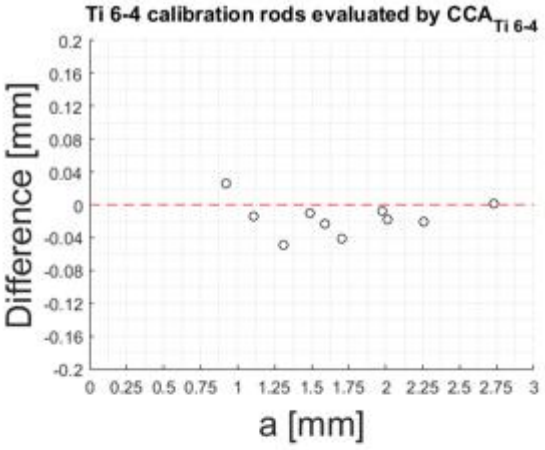
Ti 6-4 calibration rods evaluated by CCA Ti 6-4
Difference [mm]
a [mm]

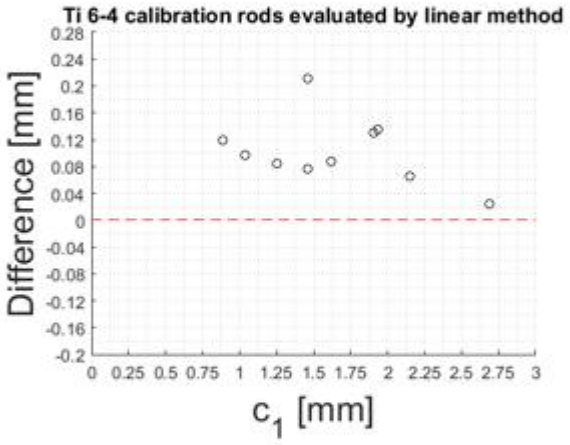
Ti 6-4 calibration rods evaluated by linear method
Difference [mm]
c1 [mm]

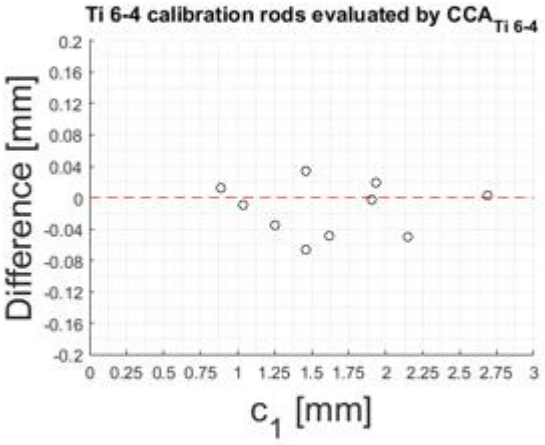
Ti 6-4 calibration rods evaluated by CCA Ti 6-4
Difference [mm]
c1 [mm]

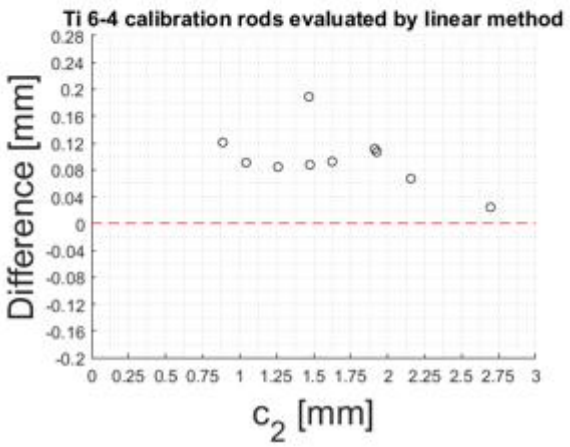
Ti 6-4 calibration rods evaluated by linear method
Difference [mm]
c2 [mm]

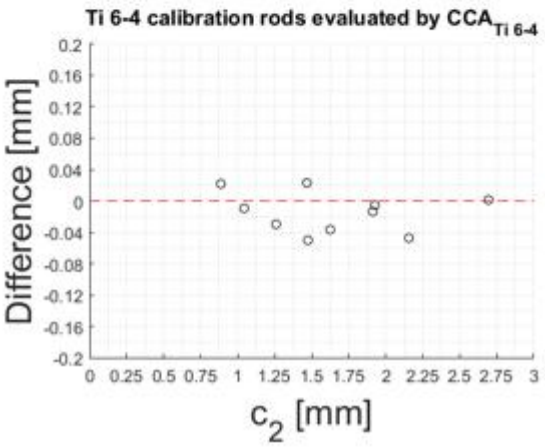
Ti 6-4 calibration rods evaluated by CCA Ti 6-4
Difference [mm]
c2 [mm]

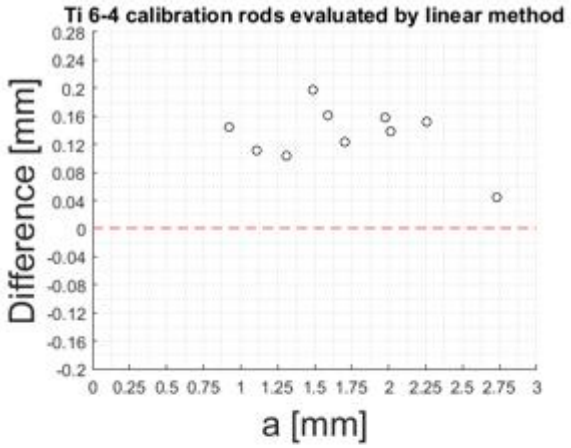
Ti 6-4 calibration rods evaluated by linear method
Difference [mm]
a [mm]

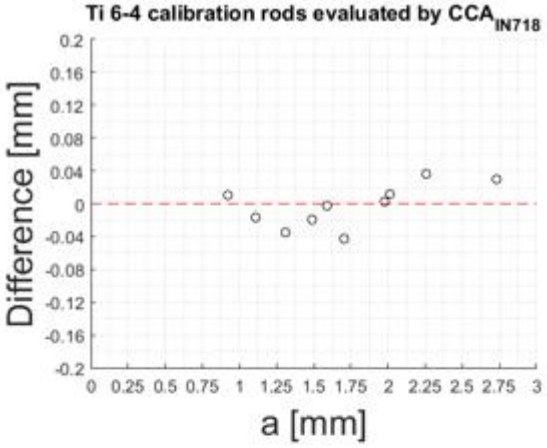
Ti 6-4 calibration rods evaluated by CCA IN718
Difference [mm]
a [mm]

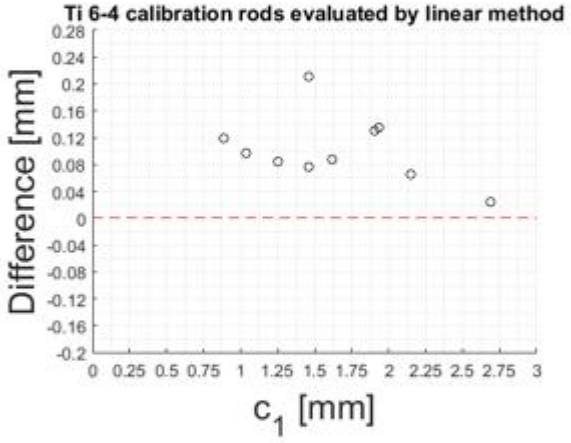
Ti 6-4 calibration rods evaluated by linear method
Difference [mm]
c1 [mm]

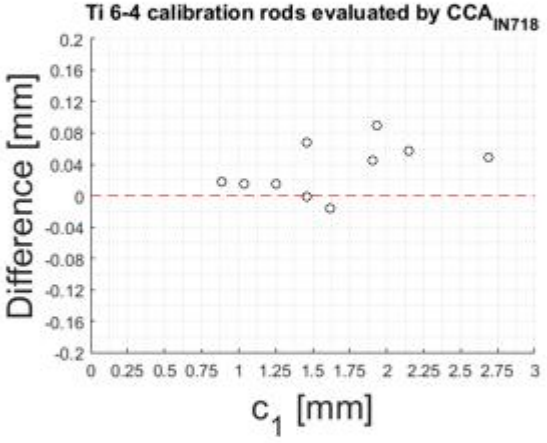
Ti 6-4 calibration rods evaluated by CCA IN718
Difference [mm]
c1 [mm]

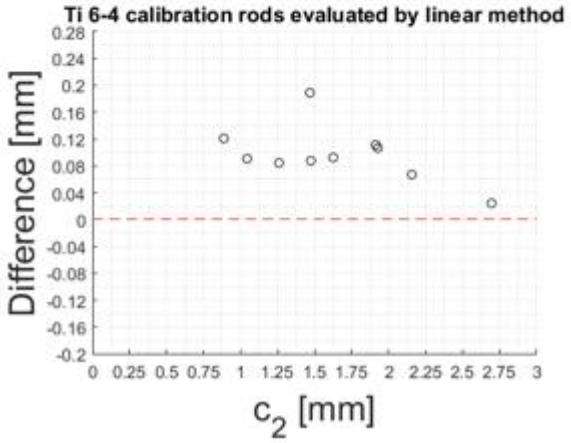
Ti 6-4 calibration rods evaluated by linear method
Difference [mm]
c2 [mm]

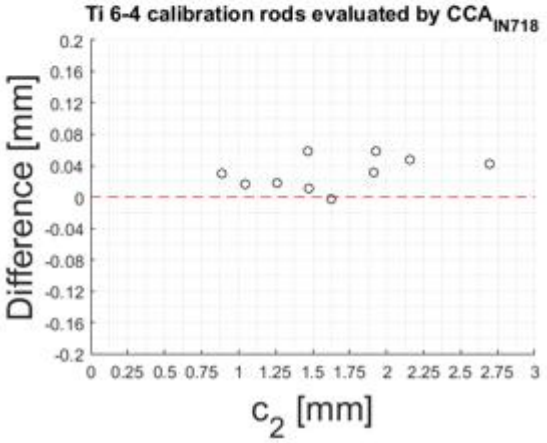
Ti 6-4 calibration rods evaluated by CCA IN718
Difference [mm]
c2 [mm]

Appendix V – Error comparison for CCA Lab A

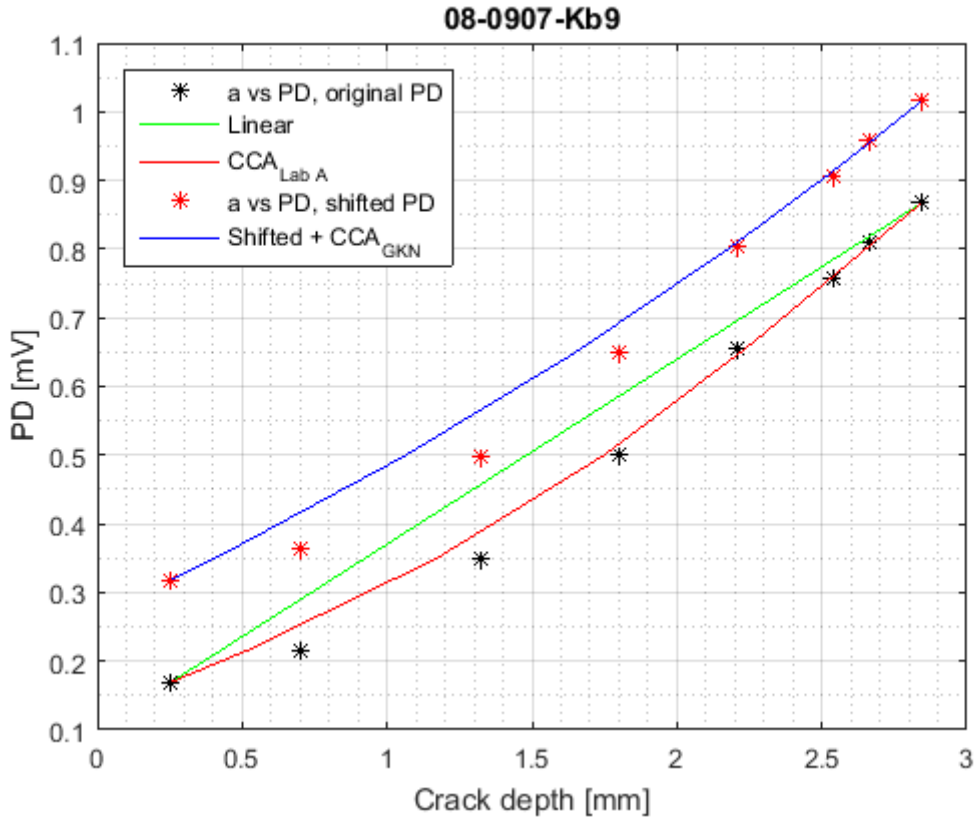

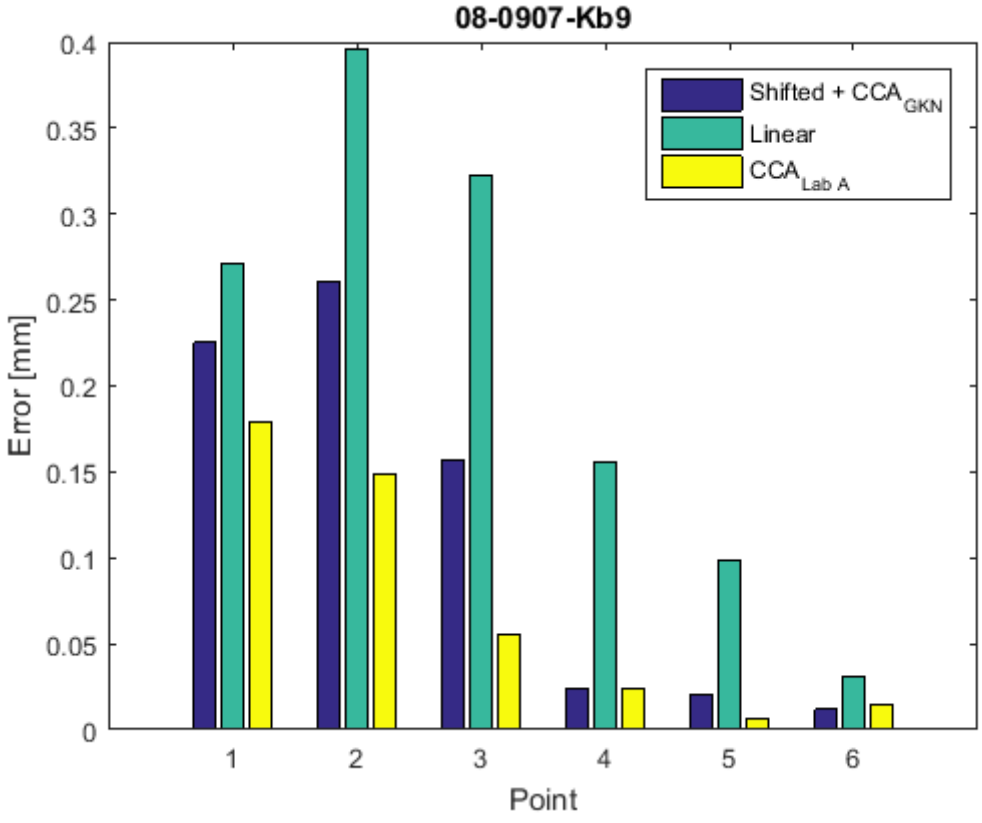

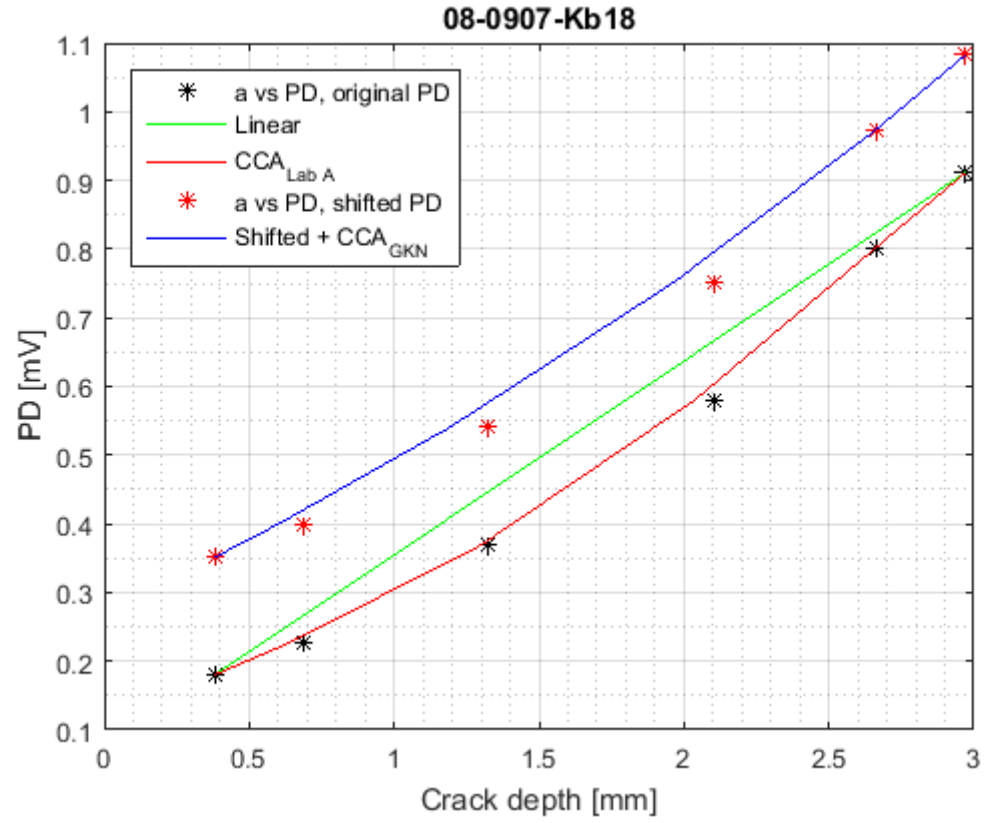
08-0907-Kb18
a vs PD, original PD
Linear
CCA Lab A
a vs PD, shifted PD
Shifted + CCA GKN
PD [mV]
Crack depth [mm]
1.1
1
0.9
0.8
0.7
0.6
0.5
0.4
0.3
0.2
0.1
0
0.5
1
1.5
2
2.5
3

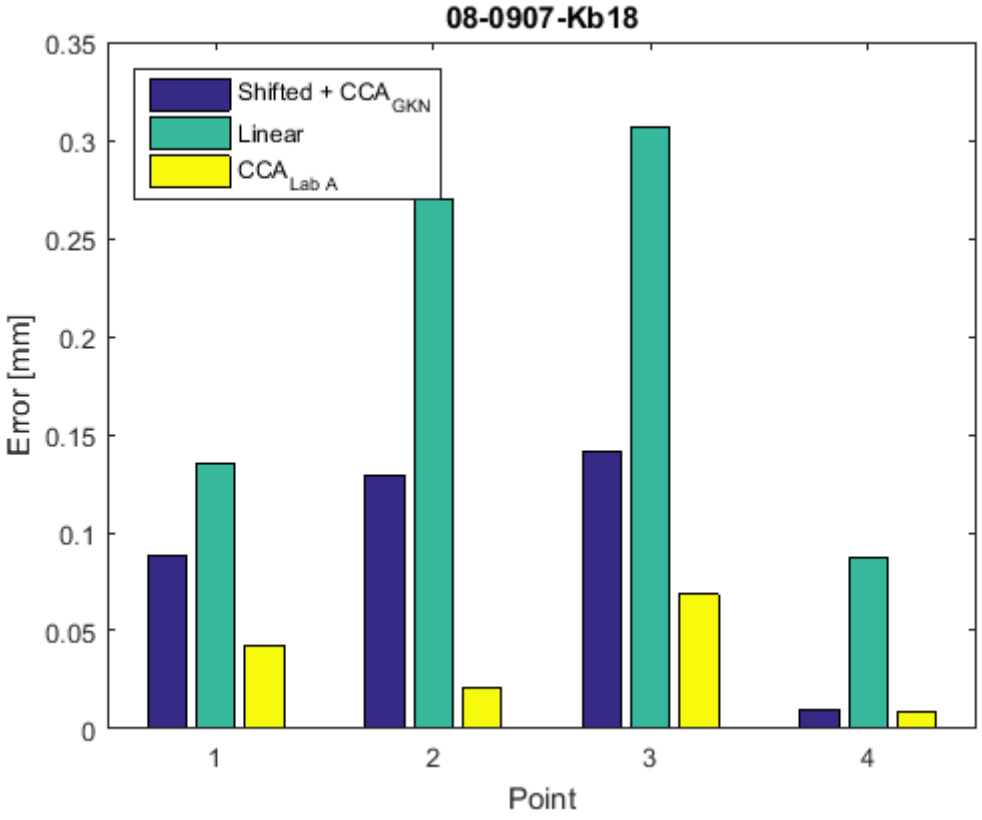
08-0907-Kb18
Shifted + CCA GKN
Linear
CCA Lab A
Error [mm]
Point
0.35
0.3
0.25
0.2
0.15
0.1
0.05
0
1
2
3
4

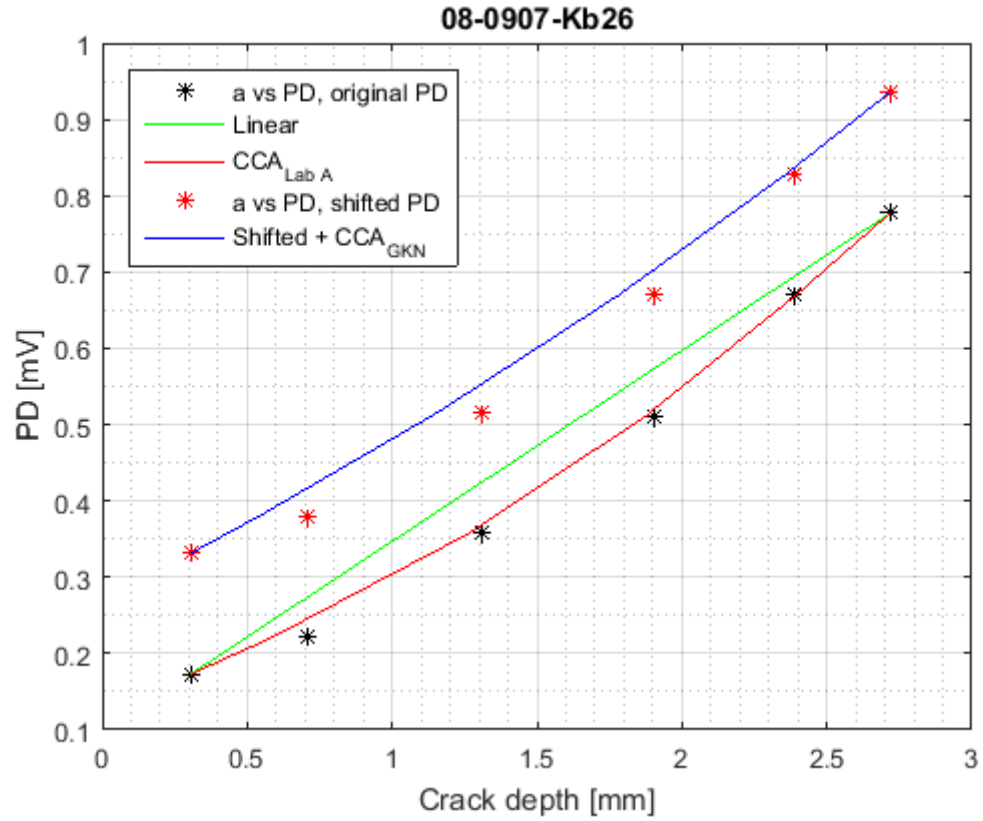
08-0907-Kb26
a vs PD, original PD
Linear
CCA Lab A
a vs PD, shifted PD
Shifted + CCA GKN
PD [mV]
Crack depth [mm]
1
0.9
0.8
0.7
0.6
0.5
0.4
0.3
0.2
0.1
0
0.5
1
1.5
2
2.5
3

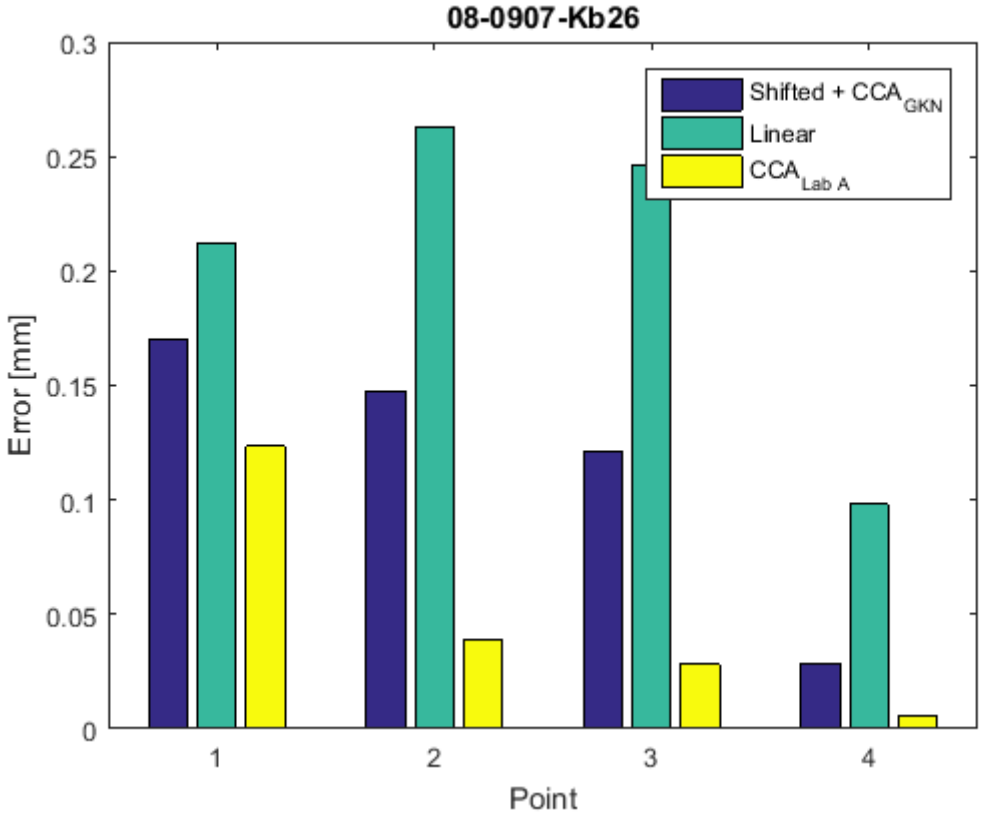
08-0907-Kb26
Shifted + CCA GKN
Linear
CCA Lab A
Error [mm]
Point
0.3
0.25
0.2
0.15
0.1
0.05
0
1
2
3
4

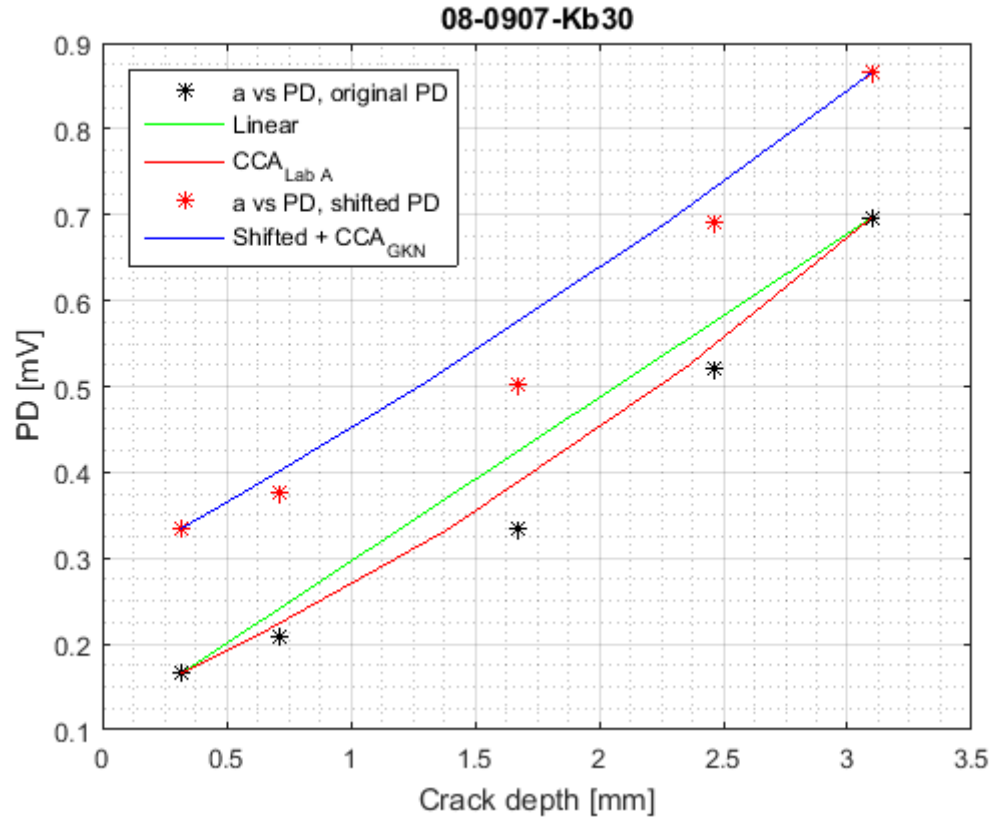
08-0907-Kb30
a vs PD, original PD
Linear
CCA Lab A
a vs PD, shifted PD
Shifted + CCA GKN
PD [mV]
Crack depth [mm]
0.9
0.8
0.7
0.6
0.5
0.4
0.3
0.2
0.1
0
0.5
1
1.5
2
2.5
3
3.5

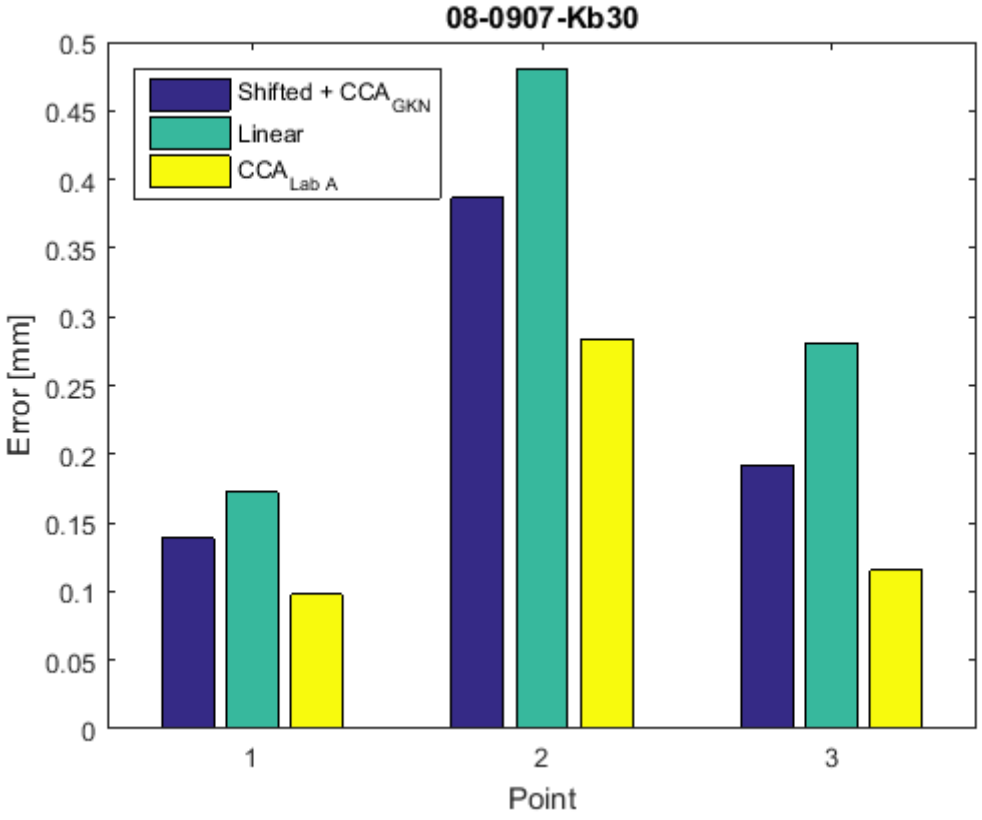
08-0907-Kb30
Shifted + CCA GKN
Linear
CCA Lab A
Error [mm]
Point
0.5
0.45
0.4
0.35
0.3
0.25
0.2
0.15
0.1
0.05
0
1
2
3

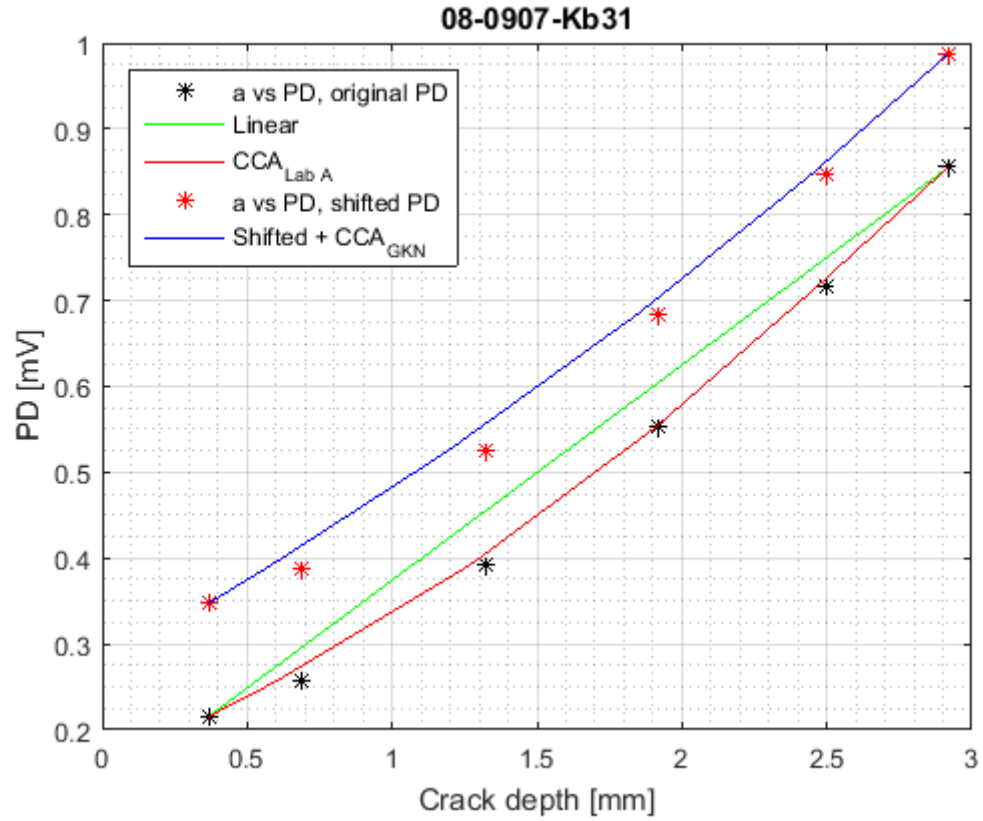
08-0907-Kb31
a vs PD, original PD
Linear
CCA Lab A
a vs PD, shifted PD
Shifted + CCA GKN
PD [mV]
Crack depth [mm]
1
0.9
0.8
0.7
0.6
0.5
0.4
0.3
0.2
0
0.5
1
1.5
2
2.5
3

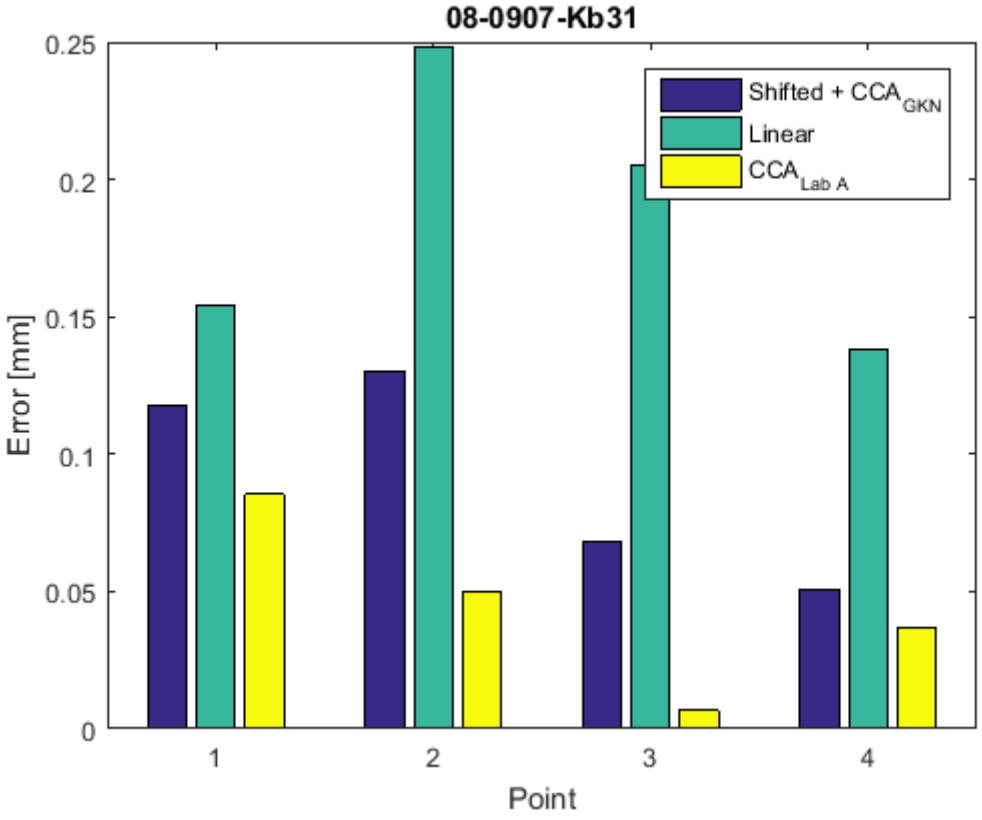
08-0907-Kb31
Shifted + CCA GKN
Linear
CCA Lab A
Error [mm]
Point
0.25
0.2
0.15
0.1
0.05
0
1
2
3
4

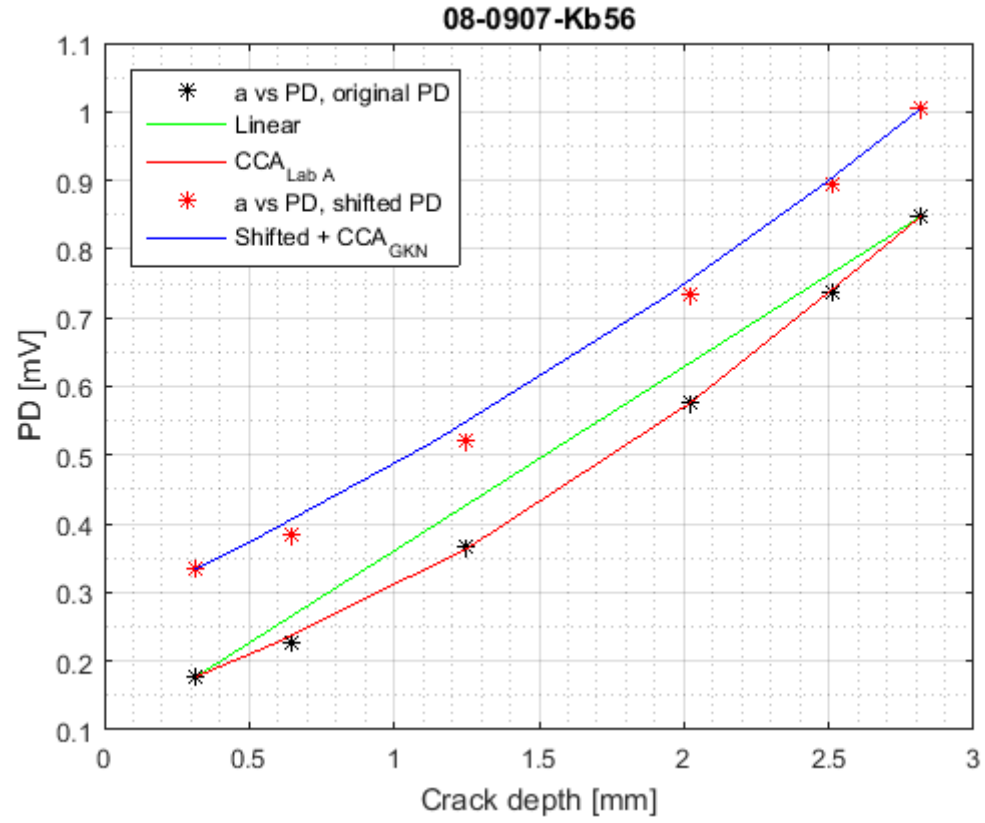
08-0907-Kb56
a vs PD, original PD
Linear
CCA Lab A
a vs PD, shifted PD
Shifted + CCA GKN
PD [mV]
Crack depth [mm]
1.1
1
0.9
0.8
0.7
0.6
0.5
0.4
0.3
0.2
0.1
0
0.5
1
1.5
2
2.5
3

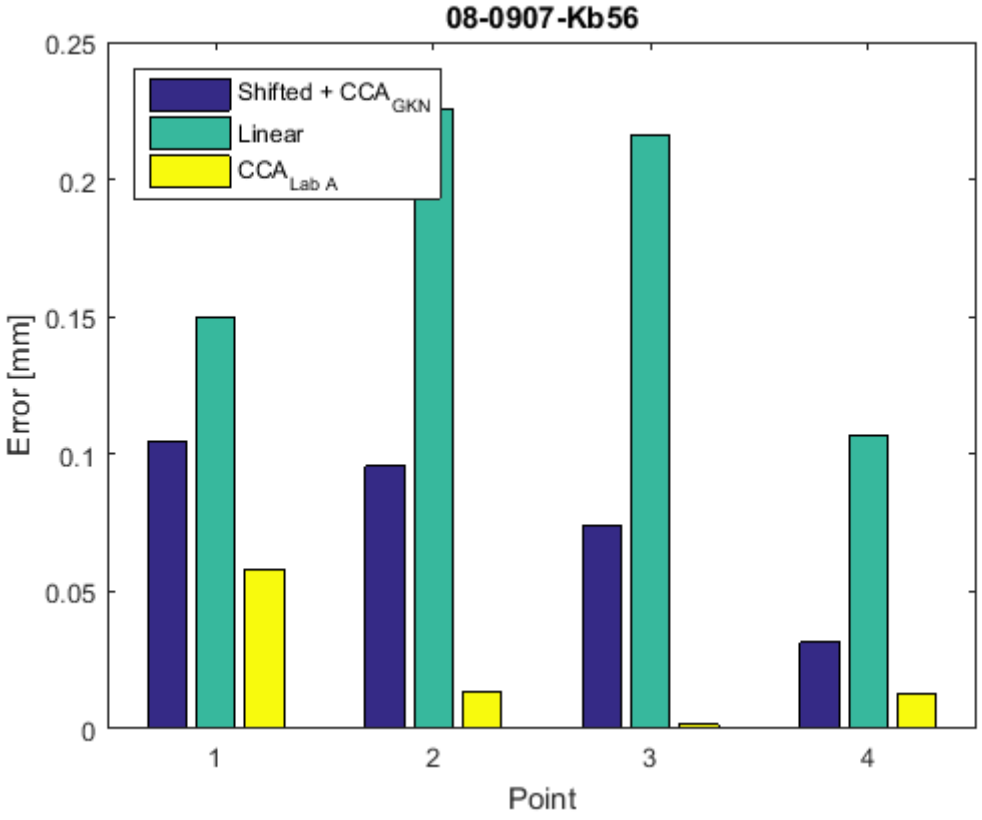
08-0907-Kb56
Shifted + CCA GKN
Linear
CCA Lab A
Error [mm]
Point
0.25
0.2
0.15
0.1
0.05
0
1
2
3
4

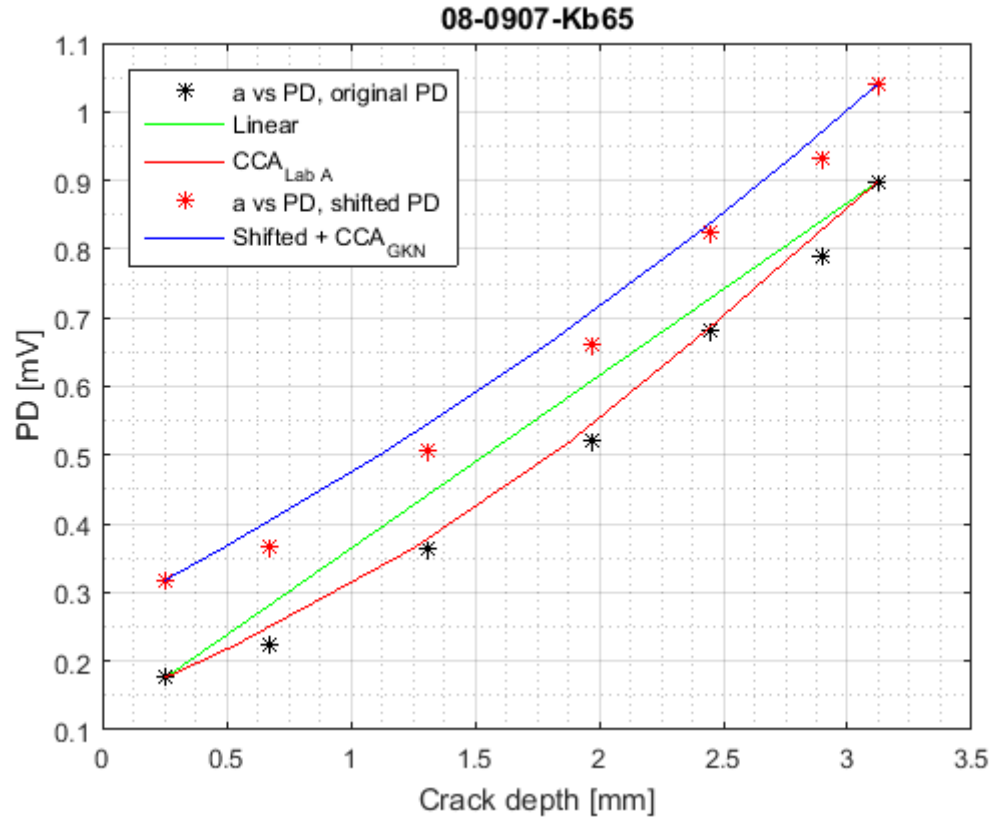
08-0907-Kb65
a vs PD, original PD
Linear
CCA Lab A
a vs PD, shifted PD
Shifted + CCA GKN
PD [mV]
Crack depth [mm]
1.1
1
0.9
0.8
0.7
0.6
0.5
0.4
0.3
0.2
0.1
0
0.5
1
1.5
2
2.5
3
3.5

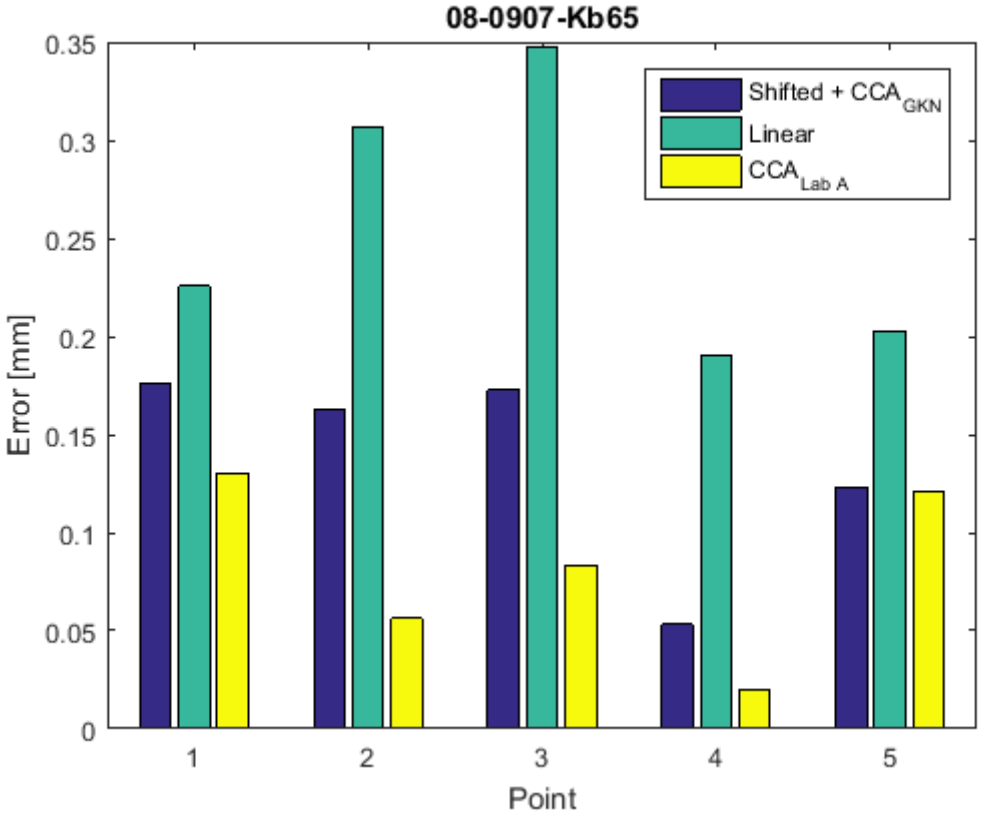
08-0907-Kb65
Shifted + CCA GKN
Linear
CCA Lab A
Error [mm]
Point
0.35
0.3
0.25
0.2
0.15
0.1
0.05
0
1
2
3
4
5

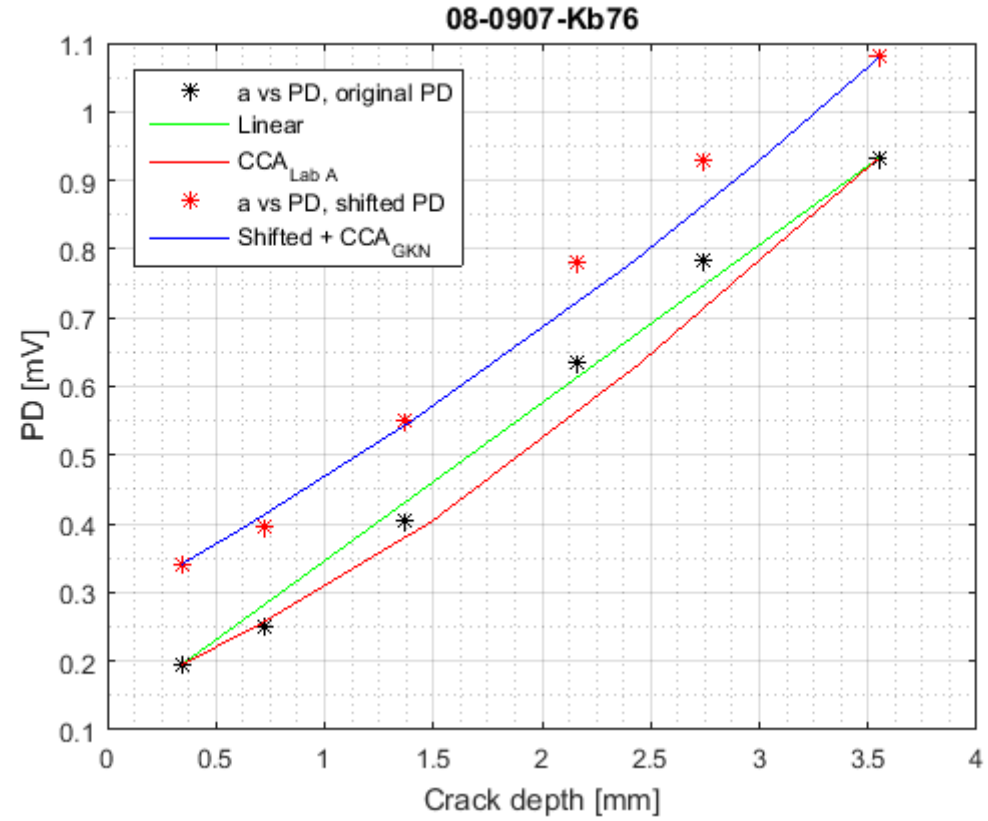
08-0907-Kb76
a vs PD, original PD
Linear
CCA Lab A
a vs PD, shifted PD
Shifted + CCA GKN
PD [mV]
Crack depth [mm]
1.1
1
0.9
0.8
0.7
0.6
0.5
0.4
0.3
0.2
0.1
0
0.5
1
1.5
2
2.5
3
3.5
4

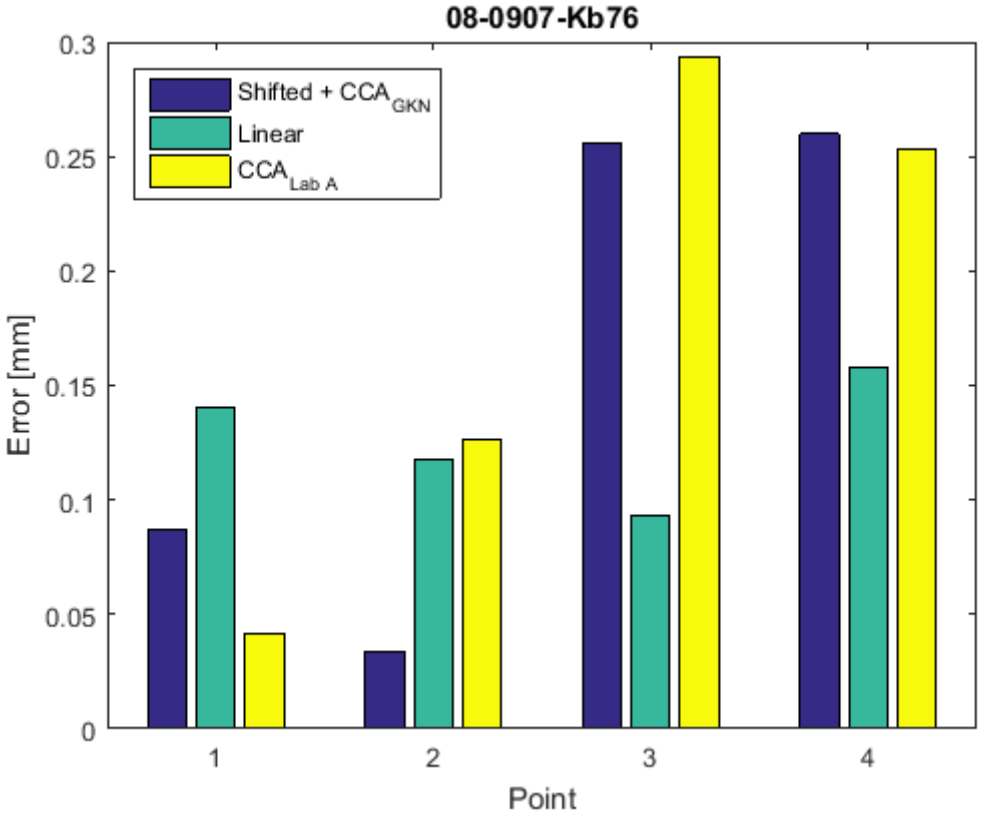
08-0907-Kb76
Shifted + CCA GKN
Linear
CCA Lab A
Error [mm]
Point
0.3
0.25
0.2
0.15
0.1
0.05
0
1
2
3
4

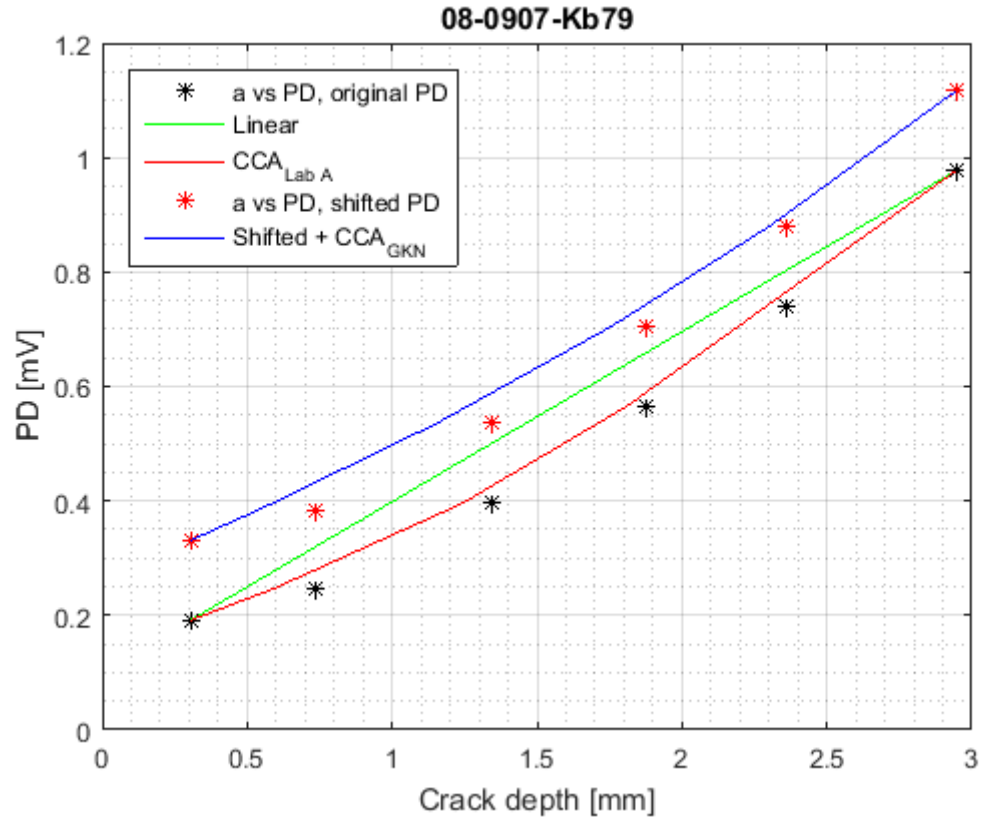
08-0907-Kb79
a vs PD, original PD
Linear
CCA Lab A
a vs PD, shifted PD
Shifted + CCA GKN
PD [mV]
Crack depth [mm]
0
0.2
0.4
0.6
0.8
1
1.2
0.5
1.5
2
2.5
3

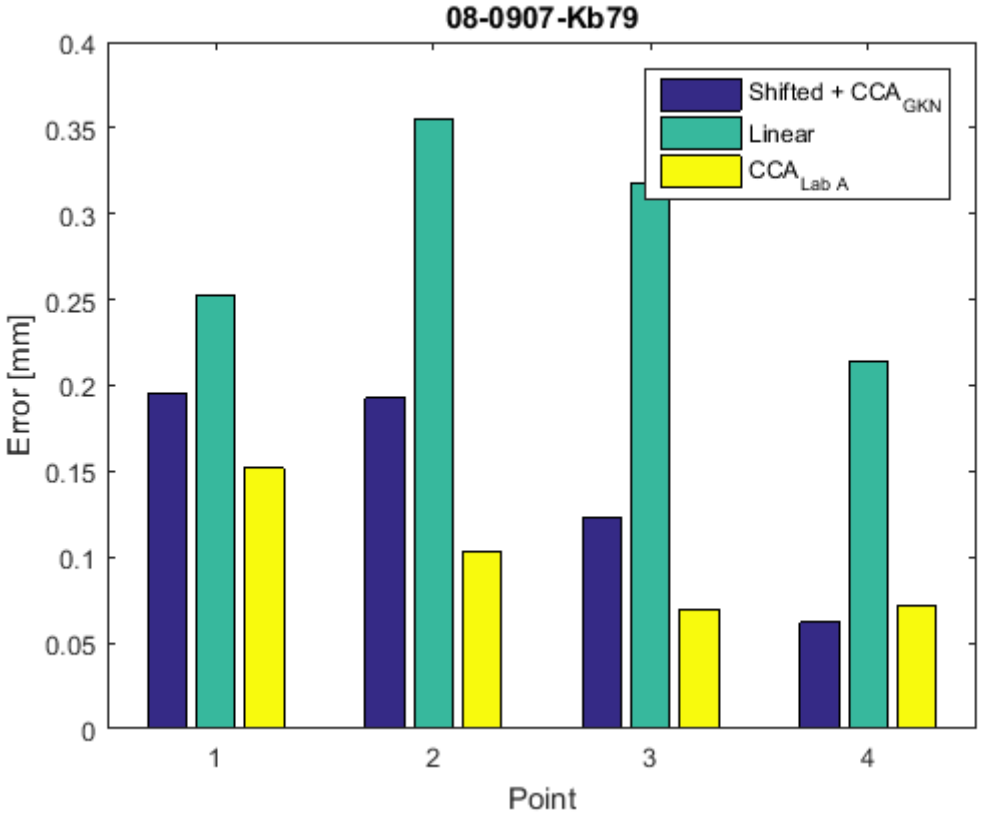
08-0907-Kb79
Shifted + CCA GKN
Linear
CCA Lab A
Error [mm]
Point
0
0.05
0.1
0.15
0.2
0.25
0.3
0.35
0.4
1
2
3
4